

Exact Prescribed-Time Prescribed-Accuracy Control for Spacecraft with Dual Reaction Wheel Saturation

First A. Author * and Second B. Author Jr.[†]

Business or Academic Affiliation 1, City, State, Zip Code

Third C. Author[‡]

Business or Academic Affiliation 2, City, Province, Zip Code, Country

Fourth D. Author[§]

Business or Academic Affiliation 2, City, State, Zip Code

This paper proposes a Timed Prescribed-Accuracy and Prescribed-Time Control (TPA-PTC) framework for rigid spacecraft equipped with reaction wheels subject to dual saturation (torque and angular-momentum limits). The proposed scheme ensures convergence to a user-prescribed accuracy at the user-specified time while strictly respecting dual saturation. It adopts a two-loop architecture: the outer loop plans a feasible reference trajectory that satisfies dual saturation and reaches the target state exactly at the user-specified terminal time, and the inner loop develops a nonsingular prescribed-time tracking controller to drive attitude and angular-velocity errors into a prescribed accuracy neighborhood before the terminal instant without gain blow-up. Meanwhile, a systematic parameter-synthesis procedure is developed to coordinate the two loops and maintain feasibility under disturbances. Numerical simulations of large-angle maneuvers in the presence of disturbances validate the proposed approach.

Nomenclature

Roman Symbols

d	lumped disturbance torque [N · m]
d_{\max}	bound on $\ d(t)\ $ [N · m]
h_w	reaction-wheel angular momentum (body frame) [kg · m ² /s]
$h_{w,i,\max}$	maximum allowable wheel momentum (axis i) [kg · m ² /s]
$h_{w,0}$	initial wheel momentum [kg · m ² /s]
H	total angular momentum, $H = J\omega + h_w$ [kg · m ² /s]

*Insert Job Title, Department Name, Address/Mail Stop, and AIAA Member Grade (if any) for first author.

[†]Insert Job Title, Department Name, Address/Mail Stop, and AIAA Member Grade (if any) for second author.

[‡]Insert Job Title, Department Name, Address/Mail Stop, and AIAA Member Grade (if any) for third author.

[§]Insert Job Title, Department Name, Address/Mail Stop, and AIAA Member Grade (if any) for fourth author (etc.).

H_{\max}	bound on $\ \mathbf{H}(t)\ $ over $[0, T_f]$ [$\text{kg} \cdot \text{m}^2/\text{s}$]
\mathbf{J}	spacecraft inertia matrix [$\text{kg} \cdot \text{m}^2$]
$\lambda_{\min}(\mathbf{J}), \lambda_{\max}(\mathbf{J})$	minimum/maximum eigenvalues of \mathbf{J} [$\text{kg} \cdot \text{m}^2$]
$\mathbf{R}(\sigma_e)$	direction cosine matrix associated with σ_e [-]
$\mathbf{G}(\sigma)$	MRP kinematic matrix [-]
T_f	user-specified terminal time [s]
T_{p1}, T_{p2}	prescribed convergence times (attitude/sliding variable) [s]
τ	control torque applied to spacecraft body [$\text{N} \cdot \text{m}$]
$\tau_{i,\max}$	maximum allowable torque (axis i) [$\text{N} \cdot \text{m}$]
τ_{ref}	planned reference torque from the outer-loop OCP [$\text{N} \cdot \text{m}$]
ω	spacecraft angular velocity (body frame) [rad/s]
ω_d	reference angular velocity [rad/s]
ω_e	angular-velocity tracking error [rad/s]
$\omega_{d,\max}$	bound on $\ \omega_d(t)\ $ on $[0, T_f]$ [rad/s]
$\dot{\omega}_{d,\max}$	bound on $\ \dot{\omega}_d(t)\ $ on $[0, T_f]$ [rad/s ²]
σ	Modified Rodrigues Parameters (MRPs) [-]
σ_d	reference MRPs [-]
σ_e	attitude tracking error in MRPs [-]
μ_i	row-sum coefficient of inertia, $\mu_i = \sum_{j=1}^3 J_{ij} $ [$\text{kg} \cdot \text{m}^2$]
λ	OCP smoothness weight in (25) [-]

Greek Symbols

η	exponent in prescribed-time law, $0 < \eta < 1$ [-]
$\varepsilon_1, \varepsilon_2$	prescribed accuracy tolerances (attitude/sliding variable) [-]
$\varepsilon_{\text{mission}}$	mission-level attitude accuracy requirement [-]
α_1, α_2	tunable gains in prescribed-time laws [-]
γ_u, γ_h	constraint-tightening margins (torque/momenta) [-]

I. Introduction

Time-critical spacecraft missions, such as rendezvous, docking, and formation reconfiguration, require the attitude to reach a commanded state at an exact user-specified terminal time T_f , which is dictated by orbital geometry, communication windows, or multi-vehicle coordination requirements [1–3]. This terminal-time requirement becomes substantially more challenging for reaction-wheel spacecraft that operate under dual reaction-wheel saturation, which

includes the torque saturation and the wheel angular-momentum saturation. For brevity, this paper refers to dual reaction-wheel saturation as dual saturation. During large-angle maneuvers, wheel momentum can saturate even when torque commands stay within bounds, which makes many analytically valid controllers physically unrealizable. Accordingly, a practical terminal-time control strategy should guarantee arrival at $t = T_f$ while strictly respecting dual saturation throughout the maneuver.

To overcome the sluggishness of asymptotic designs, finite-time control (FTC) [4?] and fixed-time control (FxTC) [5, 6] have been widely studied. FTC guarantees convergence in finite time, but the settling time depends on initial conditions, which weakens timing predictability. FxTC removes this dependence, but it typically provides a conservative upper bound that cannot be aligned with a mission-specified terminal time. These limitations motivate prescribed-time and predefined-time control, where the convergence time enters explicitly as a design parameter.

Existing prescribed-time methods can be broadly categorized into three lines. The first embeds the prescribed time into Lyapunov inequalities using exponential and power terms [7, 8] and has been applied to robotic tracking, launch-vehicle attitude control, flexible spacecraft, and formation flying [3, 9–14]. These designs are markedly conservative, often driving convergence well before the specified time and inducing very large initial torque demands. The second line employs time-varying high-gain feedback with time-warping transformations [15, 16] and has been used in consensus and robust tracking [17–19] as well as UAV tracking under saturation [20]. Compared with the first line, conservatism is reduced, but the gain typically grows rapidly as time approaches T_f , which makes the controller vulnerable to saturation and noise. In practice, truncation or smoothing is introduced to keep gains bounded [18, 21], but this comes at the cost of performance, since terminal-time tightness and tracking accuracy are generally weakened. The third line leverages periodic delayed feedback to obtain smooth prescribed-time stabilization [22–24]. Although it avoids singularities, it can be sensitive to disturbances and may induce inefficient attitude reversals, which increases momentum usage.

Despite these advances, existing PTC approaches for reaction-wheel spacecraft still exhibit two fundamental shortcomings that hinder their use in time-critical missions. First, many existing designs are conservative. They typically guarantee convergence no later than a prescribed bound, yet the closed-loop system often settles much earlier, as reported in [3] where the prescribed time is set to 500 s but the convergence occurs at about 250 s. **Such early convergence** is unacceptable for missions with hard terminal-time requirements, and it can also waste control effort or even trigger unnecessarily large torque transients, which is undesirable for reaction-wheel spacecraft.

Second, most existing studies do not explicitly consider physical realizability. **Many** PTC laws remain mathematically appealing but may demand large torque and momentum resources that cannot be delivered by reaction wheels in practice. Moreover, the terminal time for a given maneuver cannot be selected arbitrarily since it admits a lower bound determined jointly by actuator capabilities and mission demands, and dual saturation can make this lower bound particularly restrictive for large-angle maneuvers. Although some works incorporate torque saturation into the controller

design [2, 14, 20], they rarely address the minimum feasible prescribed time and typically do not treat wheel-momentum saturation in a unified manner.

Optimization-based trajectory planning can provide a potential solution because it can explicitly embed torque and momentum limits and enforce terminal-time boundary conditions by construction [25–28]. However, these approaches are often applied in an open-loop manner. Under disturbances or modeling errors, tracking can drift away from the planned trajectory and terminal-time accuracy is not guaranteed. Some studies have combined optimization with feedback control to improve practical performance [29, 30], but aggressive maneuvers and significant disturbances can still lead to noticeable deviation, and terminal-time tracking guarantees remain largely unavailable.

Motivated by these observations, this paper proposes a TPA–PTC framework built on a two-loop architecture. The outer loop plans a physically realizable reference trajectory that respects dual saturations and reaches the target state exactly at the user-specified terminal time T_f . The inner loop designs a continuous, nonsingular prescribed-time sliding-mode tracking controller, which guarantees that the spacecraft tracks the planned trajectory and drives the attitude and angular-velocity errors into a user-prescribed accuracy neighborhood before T_f , without gain blow-up. Together, the two loops ensure terminal-time attitude maneuvers that satisfy dual saturation while achieving user-specified accuracy at the mission time. In addition, a systematic parameter-synthesis procedure is provided to coordinate the two loops and maintain feasibility in the presence of disturbances.

The main contributions of this paper are summarized as follows:

- 1) A TPA–PTC framework is proposed that guarantees exact terminal-time convergence while strictly respecting dual saturation.
- 2) A continuous, nonsingular prescribed-time prescribed-accuracy tracking control law is developed to drive the attitude and angular-velocity errors into a user-prescribed accuracy neighborhood within a prescribed time, without gain blow-up.
- 3) A systematic design and parameter-synthesis procedure is provided to coordinate planning and tracking and to maintain feasibility under bounded disturbances.

The remainder of this paper is organized as follows. Section II formulates the spacecraft attitude dynamics with reaction wheels and the dual saturation constraints, and it reviews practical prescribed-time stability tools. Section III presents the proposed framework, including trajectory planning, controller design, and synthesis rules. Section IV reports simulation studies for large-angle maneuvers under significant disturbances. Section V concludes the paper and discusses future work.

II. Problem Description and Preliminaries

A. Problem Description

Let \mathbb{R} denote the set of real numbers. For vectors and matrices, $(\cdot)^T$ denotes transpose, $\|\cdot\|$ denotes the Euclidean norm, and \mathbf{I}_n denotes the $n \times n$ identity matrix. For a symmetric positive definite matrix \mathbf{A} , $\lambda_{\min}(\mathbf{A})$ and $\lambda_{\max}(\mathbf{A})$ denote its minimum and maximum eigenvalues, respectively. For any $\mathbf{a} = [a_1, a_2, a_3]^T \in \mathbb{R}^3$, define

$$\mathbf{a}^\times \triangleq \begin{bmatrix} 0 & -a_3 & a_2 \\ a_3 & 0 & -a_1 \\ -a_2 & a_1 & 0 \end{bmatrix}$$

The attitude kinematics and dynamics of a rigid spacecraft with reaction wheels can be written as

$$\dot{\boldsymbol{\sigma}} = \mathbf{G}(\boldsymbol{\sigma})\boldsymbol{\omega}, \quad \mathbf{G}(\boldsymbol{\sigma}) = \frac{1}{4} [(1 - \boldsymbol{\sigma}^T \boldsymbol{\sigma})\mathbf{I}_3 + 2\boldsymbol{\sigma}^\times + 2\boldsymbol{\sigma}\boldsymbol{\sigma}^T] \quad (1)$$

$$\mathbf{J}\dot{\boldsymbol{\omega}} + \boldsymbol{\omega}^\times(\mathbf{J}\boldsymbol{\omega} + \mathbf{h}_w) = \mathbf{d} + \boldsymbol{\tau}, \quad \boldsymbol{\tau} = -\dot{\mathbf{h}}_w \quad (2)$$

where $\boldsymbol{\sigma} \in \mathbb{R}^3$ denotes the modified Rodrigues parameters (MRPs) of the spacecraft attitude, $\boldsymbol{\omega} \in \mathbb{R}^3$ is the body angular velocity with respect to the inertial frame expressed in the body frame, $\mathbf{J} \in \mathbb{R}^{3 \times 3}$ is the constant symmetric positive definite inertia matrix, $\mathbf{h}_w \in \mathbb{R}^3$ is the reaction-wheel angular momentum expressed in the body frame, $\boldsymbol{\tau} \in \mathbb{R}^3$ is the control torque applied to the spacecraft body, and $\mathbf{d} \in \mathbb{R}^3$ denotes the lumped disturbance torque.

For clarity of exposition, a three-axis reaction-wheel cluster is considered, where the wheel axes are aligned with the body principal axes. The reaction-wheel actuators are subject to dual saturation. For each axis $i \in \{1, 2, 3\}$, the following constraints hold:

$$|\tau_i(t)| \leq \tau_{i,\max} \quad (3)$$

$$|h_{w,i}(t)| \leq h_{w,i,\max} \quad (4)$$

where τ_i and $h_{w,i}$ denote the i th components of the control torque $\boldsymbol{\tau}$ and wheel angular momentum \mathbf{h}_w , respectively, and $\tau_{i,\max} > 0$ and $h_{w,i,\max} > 0$ are the corresponding component-wise bounds.

Let $\boldsymbol{\sigma}_d \in \mathbb{R}^3$ and $\boldsymbol{\omega}_d \in \mathbb{R}^3$ denote the desired attitude MRP and angular velocity, respectively. The attitude tracking error $\boldsymbol{\sigma}_e \in \mathbb{R}^3$ is defined as the MRP representation of the relative rotation from the desired frame to the current body frame:

$$\boldsymbol{\sigma}_e = \frac{(1 - \|\boldsymbol{\sigma}_d\|^2)\boldsymbol{\sigma} - (1 - \|\boldsymbol{\sigma}\|^2)\boldsymbol{\sigma}_d + 2\boldsymbol{\sigma}_d^\times\boldsymbol{\sigma}}{1 + \|\boldsymbol{\sigma}\|^2\|\boldsymbol{\sigma}_d\|^2 + 2\boldsymbol{\sigma}^T\boldsymbol{\sigma}_d} \quad (5)$$

$$\boldsymbol{\omega}_e = \boldsymbol{\omega} - \mathbf{R}(\boldsymbol{\sigma}_e)\boldsymbol{\omega}_d \quad (6)$$

where $\mathbf{R}(\boldsymbol{\sigma}_e) \in \mathbb{R}^{3 \times 3}$ is the direction cosine matrix associated with $\boldsymbol{\sigma}_e$, given by

$$\mathbf{R}(\boldsymbol{\sigma}_e) = \mathbf{I}_3 + \frac{8\boldsymbol{\sigma}_e^\times \boldsymbol{\sigma}_e^\times - 4(1 - \boldsymbol{\sigma}_e^T \boldsymbol{\sigma}_e)\boldsymbol{\sigma}_e^\times}{(1 + \boldsymbol{\sigma}_e^T \boldsymbol{\sigma}_e)^2} \quad (7)$$

To avoid the MRP singularity at 360° , the standard shadow-set switching can be applied; hence, the error representation can be kept in the practical region $\|\boldsymbol{\sigma}_e(t)\| < 1$.

Based on the above definitions, the tracking error dynamics can be written as

$$\dot{\boldsymbol{\sigma}}_e = \mathbf{G}(\boldsymbol{\sigma}_e)\boldsymbol{\omega}_e \quad (8)$$

$$\mathbf{J}\dot{\boldsymbol{\omega}}_e = \boldsymbol{\tau} + \mathbf{d} + \mathbf{f} \quad (9)$$

where $\mathbf{f} \in \mathbb{R}^3$ is a known feedforward term determined by the measured states and the reference signals, given by

$$\mathbf{f} := -\boldsymbol{\omega}^\times(\mathbf{J}\boldsymbol{\omega} + \mathbf{h}_w) + \mathbf{J}\boldsymbol{\omega}_e^\times \mathbf{R}(\boldsymbol{\sigma}_e)\boldsymbol{\omega}_d + \mathbf{J}\mathbf{R}(\boldsymbol{\sigma}_e)\dot{\boldsymbol{\omega}}_d$$

The following assumptions are imposed.

Assumption 1. *The user-specified terminal time $T_f > 0$ satisfies*

$$T_f \geq T_{f,\min} \quad (10)$$

where $T_{f,\min} > 0$ is the minimum maneuver time required to transfer the spacecraft from the initial state to the target state under the component-wise constraints (3)–(4). Consequently, there exists a dynamically feasible reference trajectory $(\boldsymbol{\sigma}_d, \boldsymbol{\omega}_d)$ on $[0, T_f]$ with bounded angular velocity and angular acceleration: there exist known constants $\omega_{d,\max} > 0$ and $\dot{\omega}_{d,\max} > 0$ such that

$$\|\boldsymbol{\omega}_d(t)\| \leq \omega_{d,\max}, \quad \|\dot{\boldsymbol{\omega}}_d(t)\| \leq \dot{\omega}_{d,\max}, \quad \forall t \in [0, T_f] \quad (11)$$

Assumption 2. *The lumped disturbance torque \mathbf{d} is bounded. Namely, there exists a known constant $d_{\max} > 0$ such that*

$$\|\mathbf{d}(t)\| \leq d_{\max}, \quad \forall t \in [0, T_f] \quad (12)$$

Assumption 3. Let $\mathbf{H}(t) := \mathbf{J}\omega(t) + \mathbf{h}_w(t)$ denote the total angular momentum in the body frame. Assume momentum unloading/initialization is performed so that $\mathbf{H}(0) = \mathbf{0}$. The total momentum drift is induced only by external torques and can be understood as the accumulated effect of $\mathbf{d}(t)$ over time. Over the mission window $[0, T_f]$, this accumulation admits a known budget; hence there exists a known constant $H_{\max} > 0$ such that

$$\|\mathbf{H}(t)\| \leq H_{\max}, \quad \forall t \in [0, T_f]. \quad (13)$$

The control objective is to design a TPA-PTC scheme for a given terminal time $T_f > 0$ and a mission-required accuracy $\varepsilon_{\text{mission}} > 0$ such that: (i) the dual saturation constraints (3)–(4) hold for all $t \in [0, T_f]$; (ii) the spacecraft reaches the desired terminal state at $t = T_f$ by tracking the planned reference; and (iii) the tracking errors (σ_e, ω_e) enter a neighborhood of the origin with radius no larger than $\varepsilon_{\text{mission}}$ before T_f and remain bounded thereafter. The overall framework is shown in Fig. 1.

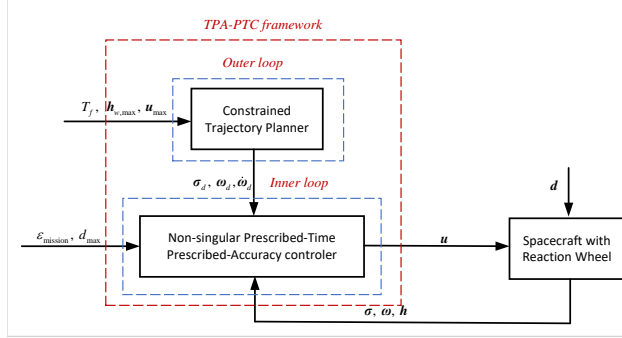


Fig. 1 The TPA-PTC framework

B. Preliminaries

This subsection summarizes basic tools on prescribed-time stability that will be used in the subsequent analysis and controller design. These results are standard and are included only for completeness.

Consider the nonlinear system

$$\dot{\mathbf{x}} = \mathbf{g}(\mathbf{x}, t) \quad (14)$$

where $\mathbf{x} \in \mathbb{R}^n$ and $\mathbf{g}(\mathbf{x}, t)$ is locally Lipschitz in \mathbf{x} , with $\mathbf{g}(\mathbf{0}, t) = \mathbf{0}$. Given a constant $T_p > 0$, the origin is said to be prescribed-time stable if, for any initial condition $\mathbf{x}(0) = \mathbf{x}_0$, the solution exists and reaches the origin in finite time $T(\mathbf{x}_0) \leq T_p$.

Lemma 1 ([9]). Suppose there exists a Lyapunov function $V(\mathbf{x})$ of system (14) such that

$$\dot{V} \leq -\frac{\pi}{\eta T_p} \left(V^{1-\frac{\eta}{2}} + V^{1+\frac{\eta}{2}} \right) \quad (15)$$

where $0 < \eta < 1$ and $T_p > 0$ are given constants. Then the state converges to the origin within time T_p , i.e., the origin is prescribed-time stable.

Theorem 1. Suppose there exists a Lyapunov function $V(\mathbf{x})$ for system (14) such that

$$\dot{V} \leq \delta V^{\frac{1}{2}} - \frac{\pi}{\eta T_p} \left[(1 + \alpha)V^{1-\frac{\eta}{2}} + V^{1+\frac{\eta}{2}} \right] \quad (16)$$

where $\delta > 0$, $\alpha > 0$, $0 < \eta < 1$, and $T_p > 0$ are constants. Then, for any initial condition, the trajectory enters the set

$$V \leq V_{\delta}^*, \quad V_{\delta}^* := \left(\frac{\delta \eta T_p}{\pi \alpha} \right)^{\frac{2}{1-\eta}} \quad (17)$$

in no more than T_p seconds and remains in it thereafter.

Proof: Let $K := \frac{\pi}{\eta T_p} > 0$ and let V_{δ}^* be defined in (17). From (16),

$$\dot{V} \leq \delta V^{\frac{1}{2}} - K \left[(1 + \alpha)V^{1-\frac{\eta}{2}} + V^{1+\frac{\eta}{2}} \right] \quad (18)$$

By construction, $V = V_{\delta}^*$ satisfies $\delta V^{1/2} = K\alpha V^{1-\eta/2}$. Moreover, for all $V \geq V_{\delta}^*$, the function $V^{-(1-\eta)/2}$ is decreasing, hence $\delta V^{1/2} \leq K\alpha V^{1-\eta/2}$, and therefore

$$\dot{V} \leq -K \left(V^{1-\frac{\eta}{2}} + V^{1+\frac{\eta}{2}} \right), \quad \forall V \geq V_{\delta}^*. \quad (19)$$

By Lemma 1, any trajectory with $V(0) > V_{\delta}^*$ reaches the set $\{V \leq V_{\delta}^*\}$ within at most T_p . Finally, note that at the boundary $V = V_{\delta}^*$ we have $\dot{V} \leq -K \left(V^{1-\frac{\eta}{2}} + V^{1+\frac{\eta}{2}} \right) < 0$, which implies that the set $\{V \leq V_{\delta}^*\}$ is forward invariant. This completes the proof. \square

The following auxiliary inequalities will be used repeatedly.

Lemma 2. For any vector $\mathbf{x} \in \mathbb{R}^n$ satisfying $\|\mathbf{x}\| \geq \varepsilon$ with $\varepsilon > 0$, and any $0 < \eta < 1$, the following inequalities hold:

$$\frac{\|\mathbf{x}\|^2}{(\|\mathbf{x}\| + \varepsilon)^\eta} \geq \frac{1}{2^\eta} \|\mathbf{x}\|^{2-\eta}, \quad \frac{\|\mathbf{x}\|^2}{(\|\mathbf{x}\| + \varepsilon)^{-\eta}} \geq \|\mathbf{x}\|^{2+\eta} \quad (20)$$

Lemma 3. The MRP attitude error kinematics are given by

$$\dot{\boldsymbol{\sigma}}_e = \mathbf{G}(\boldsymbol{\sigma}_e)\boldsymbol{\omega}_e \quad (21)$$

where $\mathbf{G}(\boldsymbol{\sigma}_e)$ is given by (1). Its spectral norm satisfies

$$\|\mathbf{G}(\boldsymbol{\sigma}_e)\| = \frac{1 + \|\boldsymbol{\sigma}_e\|^2}{4} \quad (22)$$

In particular, in the typical working region $\|\boldsymbol{\sigma}_e\| \in [0, 1]$, we have

$$\frac{1}{4} \leq \|\mathbf{G}(\boldsymbol{\sigma}_e)\| < \frac{1}{2} \quad (23)$$

Lemma 4. Let $\mathbf{J} \in \mathbb{R}^{3 \times 3}$ be a symmetric positive definite matrix with eigenvalues satisfying

$$0 < \lambda_{\min}(\mathbf{J}) \leq \lambda_{\max}(\mathbf{J})$$

Then, for any $\mathbf{x} \in \mathbb{R}^3$, it holds that

$$\lambda_{\min}(\mathbf{J})\|\mathbf{x}\|^2 \leq \mathbf{x}^T \mathbf{J} \mathbf{x} \leq \lambda_{\max}(\mathbf{J})\|\mathbf{x}\|^2 \quad (24)$$

III. Proposed TPA–PTC Framework

A. Outer-Loop Trajectory Planning Under Dual Saturation

To enforce exact arrival at the user-specified terminal time $T_f > 0$, an offline reference trajectory $(\boldsymbol{\sigma}_d(t), \boldsymbol{\omega}_d(t))$ is constructed by solving a constrained optimal control problem (OCP) over $[0, T_f]$. The OCP explicitly embeds the spacecraft kinematics and dynamics (1)–(2) together with the dual saturation constraints (3)–(4), thereby ensuring that the reference is dynamically consistent and actuator-feasible.

Specifically, the OCP is formulated as

$$\begin{aligned} \min_{\tau_{\text{ref}}(\cdot), \Delta\boldsymbol{\sigma}_0} \quad & J = \int_0^{T_f} \left(\|\boldsymbol{\tau}_{\text{ref}}(t)\|^2 + \lambda \|\dot{\boldsymbol{\tau}}_{\text{ref}}(t)\|^2 \right) dt \\ \text{s.t.} \quad & \dot{\boldsymbol{\sigma}}(t) = \mathbf{G}(\boldsymbol{\sigma}(t))\boldsymbol{\omega}(t), \\ & \mathbf{J}\dot{\boldsymbol{\omega}}(t) + \boldsymbol{\omega}(t)^{\times}(\mathbf{J}\boldsymbol{\omega}(t) + \mathbf{h}_w(t)) = \boldsymbol{\tau}_{\text{ref}}(t), \\ & \dot{\mathbf{h}}_w(t) = -\boldsymbol{\tau}_{\text{ref}}(t), \quad \mathbf{h}_w(0) = \mathbf{h}_{w,0}, \\ & \boldsymbol{\sigma}(0) = \boldsymbol{\sigma}_0, \\ & \boldsymbol{\omega}(0) = \boldsymbol{\omega}_0, \\ & \boldsymbol{\sigma}(T_f) = \boldsymbol{\sigma}_{\text{target}}, \quad \boldsymbol{\omega}(T_f) = \boldsymbol{\omega}_{\text{target}}, \\ & |\tau_{\text{ref},i}(t)| \leq (1 - \gamma_u) \tau_{i,\text{max}}, \quad i \in \{1, 2, 3\}, \\ & |h_{w,i}(t)| \leq (1 - \gamma_h) h_{w,i,\text{max}}, \quad i \in \{1, 2, 3\}. \end{aligned} \quad (25)$$

Here $\lambda > 0$ weights control effort and smoothness, while $\gamma_u, \gamma_h \in (0, 1)$ tighten the actuator bounds to reserve headroom for inner-loop tracking and disturbance rejection.

The OCP is solved offline using the Gauss pseudospectral method GPOPS-II [31], producing nodal torques $\{\boldsymbol{\tau}_i\}_{i=0}^N$ at nodes $\{t_i\}_{i=0}^N$. A continuous-time torque command is obtained via piecewise-linear interpolation:

$$\tilde{\boldsymbol{\tau}}(t) = \boldsymbol{\tau}_i + \frac{t - t_i}{t_{i+1} - t_i} (\boldsymbol{\tau}_{i+1} - \boldsymbol{\tau}_i), \quad t \in [t_i, t_{i+1}], \quad i = 0, \dots, N-1. \quad (26)$$

The interpolated torque $\tilde{\boldsymbol{\tau}}(t)$ is then integrated through (1)–(2) to reconstruct a dynamically consistent reference trajectory $(\boldsymbol{\sigma}_d(t), \boldsymbol{\omega}_d(t))$. Since each component satisfies $|\boldsymbol{\tau}_i(t_i)| \leq (1 - \gamma_u)\tau_{i,\max}$ and $|\boldsymbol{\tau}_i(t_{i+1})| \leq (1 - \gamma_u)\tau_{i,\max}$, the piecewise-linear interpolation implies $|\tilde{\boldsymbol{\tau}}_i(t)| \leq (1 - \gamma_u)\tau_{i,\max}$ for all $t \in [t_i, t_{i+1}]$.

Remark 1. *The outer-loop planner is not posed as a standalone contribution in optimal control. Its role is to embed the dual saturation limits and terminal boundary conditions into reference generation, providing a physically realizable, time-anchored trajectory for the inner-loop prescribed-time tracker.*

Remark 2. *Assumption 1 implies the existence of a minimum feasible maneuver time T_f,\min under the dual saturation constraints. A conservative estimate can be obtained via a bang-bang (time-optimal) construction under component-wise torque limits; an explicit procedure is provided in Appendix A.*

B. Inner-Loop Nonsingular Prescribed-Time Tracking Control

To facilitate a nonsingular prescribed-accuracy prescribed-time design, this section introduces the following sliding surface that couples the attitude and angular-velocity tracking errors.

Define the sliding surface as

$$\mathbf{s} = \boldsymbol{\omega}_e + \mathbf{Q}(\boldsymbol{\sigma}_e), \quad (27)$$

where

$$\mathbf{Q}(\boldsymbol{\sigma}_e) = c_1 k_1 \frac{\boldsymbol{\sigma}_e}{(\|\boldsymbol{\sigma}_e\| + \varepsilon_1)^\eta} + c_1 k_2 \frac{\boldsymbol{\sigma}_e}{(\|\boldsymbol{\sigma}_e\| + \varepsilon_1)^{-\eta}}, \quad (28)$$

with constants $0 < \eta < 1$, $\varepsilon_1 > 0$,

$$c_1 = \frac{\pi}{\eta T_{p1}}, \quad k_1 = (1 + \alpha_1)2^{1+\frac{3}{2}\eta}, \quad k_2 = 2^{1-\frac{\eta}{2}},$$

where $T_{p1} > 0$ and $\alpha_1 > 0$.

Theorem 2 (Convergence of the Attitude Error). *Suppose there exists a time $t_s \geq 0$ such that $\|\mathbf{s}(t)\| \leq s_{\max}$ for all*

$t \geq t_s$. Then the attitude error $\sigma_e(t)$ enters, within T_{p1} seconds after t_s , the bounded set

$$\|\sigma_e(t)\| \leq \max \{\varepsilon_{\delta_1}, \varepsilon_1\}, \quad \forall t \geq t_s + T_{p1}, \quad (29)$$

where

$$\varepsilon_{\delta_1} := \sqrt{2} \left(\frac{\delta_1 \eta T_{p1}}{\pi \alpha_1} \right)^{\frac{1}{1-\eta}}, \quad \delta_1 := \frac{\sqrt{2}}{2} s_{\max}. \quad (30)$$

Proof. Consider the Lyapunov function candidate

$$V_1 = \frac{1}{2} \|\sigma_e\|^2. \quad (31)$$

For t such that $\|s(t)\| \leq s_{\max}$, differentiating along the error kinematics $\dot{\sigma}_e = \mathbf{G}(\sigma_e) \omega_e$ and substituting $\omega_e = s - \mathbf{Q}(\sigma_e)$ yields

$$\begin{aligned} \dot{V}_1 &= \sigma_e^\top \mathbf{G}(\sigma_e) (s - \mathbf{Q}(\sigma_e)) \\ &\leq \|\mathbf{G}(\sigma_e)\| \|\sigma_e\| s_{\max} - \sigma_e^\top \mathbf{G}(\sigma_e) \mathbf{Q}(\sigma_e). \end{aligned} \quad (32)$$

From Lemma 3, $\|\mathbf{G}(\sigma_e)\| < \frac{1}{2}$ for $\|\sigma_e\| < 1$. Assuming $\|\sigma_e\| \geq \varepsilon_1$, Lemma 2 gives

$$\frac{\|\sigma_e\|^2}{(\|\sigma_e\| + \varepsilon_1)^\eta} \geq \frac{1}{2^\eta} \|\sigma_e\|^{2-\eta}, \quad \frac{\|\sigma_e\|^2}{(\|\sigma_e\| + \varepsilon_1)^{-\eta}} \geq \|\sigma_e\|^{2+\eta}.$$

Thus,

$$\begin{aligned} \dot{V}_1 &\leq \frac{1}{2} \|\sigma_e\| s_{\max} - \frac{c_1}{4} \left[k_1 \frac{\|\sigma_e\|^2}{(\|\sigma_e\| + \varepsilon_1)^\eta} + k_2 \frac{\|\sigma_e\|^2}{(\|\sigma_e\| + \varepsilon_1)^{-\eta}} \right] \\ &\leq \frac{\sqrt{2}}{2} V_1^{1/2} s_{\max} - \frac{c_1}{4} \left[k_1 2^{-\eta} (2V_1)^{1-\eta/2} + k_2 (2V_1)^{1+\eta/2} \right]. \end{aligned} \quad (33)$$

Substituting $c_1 = \frac{\pi}{\eta T_{p1}}$, $k_1 = (1 + \alpha_1) 2^{1+\frac{3}{2}\eta}$, and $k_2 = 2^{1-\frac{\eta}{2}}$ yields

$$\dot{V}_1 \leq \delta_1 V_1^{1/2} - \frac{\pi}{\eta T_{p1}} \left[(1 + \alpha_1) V_1^{1-\eta/2} + V_1^{1+\eta/2} \right]. \quad (34)$$

This satisfies the condition of Theorem 1. Hence, $V_1(t)$ converges within time T_{p1} to

$$V_1 \leq \frac{1}{2} \varepsilon_{\delta_1}^2. \quad (35)$$

Since $V_1 = \frac{1}{2} \|\sigma_e\|^2$, it follows that $\|\sigma_e(t)\| \leq \varepsilon_{\delta_1}$. Moreover, the regularization ensures that the set $\{\|\sigma_e\| \leq \varepsilon_1\}$ is

positively invariant. Combining both cases yields the stated bound. \square

Remark 3. The parameter ε_{δ_1} depends inversely on $\alpha_1^{1/(1-\eta)}$. Therefore, for any fixed s_{\max} and T_{p1} , one can always choose a appropriate $\alpha_1 > 0$ such that $\varepsilon_{\delta_1} < \varepsilon_1$. In this case, the ultimate convergence bound becomes $\|\sigma_e(t)\| \leq \varepsilon_1$, and the user-specified tolerance ε_1 fully determines the practical accuracy of the maneuver.

Remark 4. The parameter $\varepsilon_1 > 0$ serves two purposes: (i) it eliminates the singularity in $\mathbf{Q}(\sigma_e)$ as $\|\sigma_e\| \rightarrow 0$, ensuring a smooth and bounded control law; and (ii) it provides a direct, user-adjustable interface for specifying the desired convergence tolerance. In practical applications, exact zero error is neither achievable nor necessary; ε_1 allows engineers to encode mission-level precision requirements directly into the controller design.

Based on the above surface, construct a prescribed-time inner-loop torque command consisting of a computable feedforward cancellation term and a dominant prescribed-time stabilizing term. The resulting inner-loop control law is given by

$$\boldsymbol{\tau} = -\mathbf{f}(t) - \mathbf{J}\dot{\mathbf{Q}}(\sigma_e) + \boldsymbol{\tau}_c, \quad (36)$$

where $\mathbf{f}(t)$ is the known nonlinear term defined in (9), and the prescribed-time dominant term $\boldsymbol{\tau}_c$ is given by

$$\boldsymbol{\tau}_c = -c_2 \left[k_3 \frac{s}{(\|s\| + \varepsilon_2)^{\eta}} + k_4 \frac{s}{(\|s\| + \varepsilon_2)^{-\eta}} \right], \quad (37)$$

with design parameters $0 < \eta < 1$, $\varepsilon_2 > 0$, and

$$c_2 = \frac{\pi}{\eta T_{p2}}, \quad k_3 = (1 + \alpha_2) 2^{-1+\frac{3}{2}\eta} \lambda_{\max}(\mathbf{J})^{1-\frac{\eta}{2}}, \quad k_4 = 2^{-1-\frac{\eta}{2}} \lambda_{\max}(\mathbf{J})^{1+\frac{\eta}{2}}.$$

Here, $T_{p2} > 0$ is the prescribed convergence time for the sliding surface, and $\alpha_2 > 0$ is a tunable gain.

Substituting the control law into the attitude error dynamics (9) and using the definition of s , the closed-loop sliding surface dynamics are obtained. Left-multiplying by \mathbf{J} yields

$$\mathbf{J}\dot{s} = \boldsymbol{\tau}_c + \mathbf{d}(t), \quad (38)$$

where the lumped disturbance $\mathbf{d}(t)$ satisfies $\|\mathbf{d}(t)\| \leq d_{\max}$ as stated in Assumption 2.

Theorem 3 (Convergence of the Sliding Surface). *Suppose $\|\mathbf{d}(t)\| \leq d_{\max}$. Then the sliding variable $s(t)$ converges within time T_{p2} to the bounded set*

$$\|s(t)\| \leq \max \{\varepsilon_{\delta_2}, \varepsilon_2\}, \quad (39)$$

where

$$\varepsilon_{\delta_2} := \sqrt{2} \left(\frac{\delta_2 \eta T_{p2}}{\pi \alpha_2} \right)^{\frac{1}{1-\eta}}, \quad \delta_2 := d_{\max} \sqrt{\frac{2}{\lambda_{\min}(\mathbf{J})}}. \quad (40)$$

Proof. Define the Lyapunov function

$$V_2 = \frac{1}{2} \mathbf{s}^\top \mathbf{J} \mathbf{s}. \quad (41)$$

Its time derivative along the closed-loop dynamics is

$$\dot{V}_2 = \mathbf{s}^\top \boldsymbol{\tau}_c + \mathbf{s}^\top \mathbf{d}(t). \quad (42)$$

For the disturbance term, Lemma 4 gives

$$\mathbf{s}^\top \mathbf{d}(t) \leq \|\mathbf{s}\| d_{\max} \leq d_{\max} \sqrt{\frac{2}{\lambda_{\min}(\mathbf{J})}} V_2^{1/2} = \delta_2 V_2^{1/2}. \quad (43)$$

For the control term, applying Lemma 2 yields

$$\mathbf{s}^\top \boldsymbol{\tau}_c \leq -\frac{\pi}{\eta T_{p2}} \left[(1 + \alpha_2) V_2^{1-\frac{\eta}{2}} + V_2^{1+\frac{\eta}{2}} \right]. \quad (44)$$

Thus,

$$\dot{V}_2 \leq \delta_2 V_2^{1/2} - \frac{\pi}{\eta T_{p2}} \left[(1 + \alpha_2) V_2^{1-\frac{\eta}{2}} + V_2^{1+\frac{\eta}{2}} \right], \quad (45)$$

which satisfies the condition of Theorem 1. Hence, $V_2(t)$ converges within T_{p2} to $V_2 \leq \frac{1}{2} \varepsilon_{\delta_2}^2$. Since $V_2 \geq \frac{1}{2} \lambda_{\min}(\mathbf{J}) \|\mathbf{s}\|^2$,

it follows that

$$\|\mathbf{s}(t)\| \leq \sqrt{\frac{2}{\lambda_{\min}(\mathbf{J})}} \sqrt{V_2(t)} \leq \sqrt{2} \left(\frac{\delta_2 \eta T_{p2}}{\pi \alpha_2} \right)^{\frac{1}{1-\eta}} = \varepsilon_{\delta_2}. \quad (46)$$

The regularization ensures that the set $\{\|\mathbf{s}\| \leq \varepsilon_2\}$ is positively invariant. Combining both cases gives the result. \square

Remark 5. By selecting an appropriate value of $\alpha_2 > 0$ in conjunction with ε_2 , the designer can ensure $\varepsilon_{\delta_2} \leq \varepsilon_2$, so that the ultimate bound on the sliding surface is governed by the user-specified tolerance ε_2 . This avoids unnecessarily large control gains while achieving the desired steady-state tracking precision.

Remark 6. The inner-loop convergence occurs in two stages. First, Theorem 3 guarantees that $\|\mathbf{s}(t)\| \leq \max\{\varepsilon_{\delta_2}, \varepsilon_2\}$ for all $t \geq T_{p2}$. Let $t_s := T_{p2}$ and set $s_{\max} := \max\{\varepsilon_{\delta_2}, \varepsilon_2\}$. Then Theorem 2 implies that $\boldsymbol{\sigma}_e(t)$ enters $\|\boldsymbol{\sigma}_e\| \leq \max\{\varepsilon_{\delta_1}, \varepsilon_1\}$ for all $t \geq T_{p2} + T_{p1}$. Therefore, it suffices to require $T_{p1} + T_{p2} < T_f$ to ensure the tracking errors settle before the terminal time.

The computable feedforward term $f(t)$ in (9) can be decomposed as

$$f(t) = \tau_{\text{ref}}(t) + \Delta_f(t), \quad (47)$$

where $\Delta_f(t) := f(t) - \tau_{\text{ref}}(t)$ and its component-wise bound is given in Appendix B. The planner enforces $|\tau_{\text{ref},i}(t)| \leq (1 - \gamma_u)\tau_{i,\max}$ on $[0, T_f]$.

Theorem 4. Consider the inner-loop control law (36). Assume that along the closed-loop trajectory over $[0, T_f]$ the tracking errors remain inside the prescribed-accuracy tube, namely,

$$\|\sigma_e(t)\| \leq \varepsilon_1, \quad \|s(t)\| \leq \varepsilon_2, \quad \forall t \in [0, T_f]. \quad (48)$$

If the safety margin γ_u and prescribed-accuracy set $(\varepsilon_1, \varepsilon_2)$ are selected such that

$$\Delta_{f,i,\max}(\varepsilon_1, \varepsilon_2) + \overline{(J\dot{Q})}_i(\varepsilon_1, \varepsilon_2) + \bar{\tau}_c(\varepsilon_2) \leq \gamma_u \tau_{i,\max}, \quad i = 1, 2, 3, \quad (49)$$

where $\Delta_{f,i,\max}(\varepsilon_1, \varepsilon_2)$, $\overline{(J\dot{Q})}_i(\varepsilon_1, \varepsilon_2)$, and $\bar{\tau}_c(\varepsilon_2)$ are explicit bounds derived in the proof. Then the actuator torques satisfy $|\tau_i(t)| \leq \tau_{i,\max}$ for all $t \in [0, T_f]$ and all $i = 1, 2, 3$.

Proof. Since the maneuver is initialized consistently with the planned reference, i.e., $\sigma(0) = \sigma_d(0)$ (hence $\sigma_e(0) = \mathbf{0}$), and the prescribed-time tracking design guarantees practical convergence and tube invariance by Theorems 2–3 under proper parameter selection, the closed-loop tracking errors remain inside the prescribed-accuracy set:

$$\|\sigma_e(t)\| \leq \varepsilon_1, \quad \|s(t)\| \leq \varepsilon_2, \quad \forall t \in [0, T_f]. \quad (50)$$

On the tube (50), $\omega_e = s - Q(\sigma_e)$ implies

$$\|\omega_e(t)\| \leq \varepsilon_2 + \bar{Q}, \quad \bar{Q} := \sup_{\|\sigma_e\| \leq \varepsilon_1} \|Q(\sigma_e)\| \leq c_1 \left(k_1 2^{-\eta} \varepsilon_1^{1-\eta} + k_2 2^\eta \varepsilon_1^{1+\eta} \right). \quad (51)$$

From (36) and (47), for each axis i ,

$$|\tau_i| \leq |\tau_{\text{ref},i}| + |\Delta_{f,i}| + |(J\dot{Q})_i| + |\tau_{c,i}|. \quad (52)$$

By the planner tightening, $|\tau_{\text{ref},i}| \leq (1 - \gamma_u)\tau_{i,\max}$.

(i) *Bound on $|\Delta_{f,i}|$.* Appendix B yields, for $i = 1, 2, 3$,

$$|\Delta_{f,i}(t)| \leq (\|\omega_e(t)\| + \|\omega_d(t)\|) H_{\max} + \mu_i \|\omega_e(t)\| \|\omega_d(t)\| + 4\mu_i \|\sigma_e(t)\| \|\dot{\omega}_d(t)\|, \quad (53)$$

where $\mu_i := \sum_{j=1}^3 |J_{ij}|$ and H_{\max} is given in Assumption 3. Using (50), (51), and (11), we obtain

$$|\Delta_{f,i}(t)| \leq \Delta_{f,i,\max}(\varepsilon_1, \varepsilon_2), \quad (54)$$

with

$$\Delta_{f,i,\max}(\varepsilon_1, \varepsilon_2) := (\varepsilon_2 + \bar{Q} + \omega_{d,\max}) H_{\max} + \mu_i (\varepsilon_2 + \bar{Q}) \omega_{d,\max} + 4\mu_i \varepsilon_1 \dot{\omega}_{d,\max}. \quad (55)$$

(ii) *Bound on $|\tau_{c,i}|$.* Since $\|s(t)\| \leq \varepsilon_2$,

$$|\tau_{c,i}(t)| \leq \bar{\tau}_c(\varepsilon_2), \quad \bar{\tau}_c(\varepsilon_2) := c_2 \left(k_3 2^{-\eta} \varepsilon_2^{1-\eta} + k_4 2^\eta \varepsilon_2^{1+\eta} \right). \quad (56)$$

(iii) *Bound on $|(J\dot{Q})_i|$.* By $\dot{Q} = \frac{\partial Q}{\partial \sigma_e} G(\sigma_e) \omega_e$ and Lemma 3,

$$\|\dot{Q}(t)\| \leq \left\| \frac{\partial Q}{\partial \sigma_e} \right\| \frac{1 + \varepsilon_1^2}{4} (\varepsilon_2 + \bar{Q}).$$

Moreover, for $\rho := \|\sigma_e\| \leq \varepsilon_1$, a convenient Jacobian envelope is

$$\left\| \frac{\partial Q}{\partial \sigma_e} \right\| \leq \Psi(\varepsilon_1), \quad \Psi(\rho) := c_1 \left[k_1 (\rho + \varepsilon_1)^{-\eta} + k_2 (\rho + \varepsilon_1)^\eta + \rho (k_1 \eta (\rho + \varepsilon_1)^{-\eta-1} + k_2 \eta (\rho + \varepsilon_1)^{\eta-1}) \right]. \quad (57)$$

Let $\mu_i := \sum_{j=1}^3 |J_{ij}|$, then $|(Jv)_i| \leq \mu_i \|v\|$, and hence

$$|(J\dot{Q}(t))_i| \leq \overline{(J\dot{Q})}_i(\varepsilon_1, \varepsilon_2), \quad \overline{(J\dot{Q})}_i := \mu_i \Psi(\varepsilon_1) \frac{1 + \varepsilon_1^2}{4} (\varepsilon_2 + \bar{Q}). \quad (58)$$

Finally, substituting the bounds (i)–(iii) into (52) yields

$$|\tau_i(t)| \leq (1 - \gamma_u) \tau_{i,\max} + \Delta_{f,i,\max}(\varepsilon_1, \varepsilon_2) + \overline{(J\dot{Q})}_i(\varepsilon_1, \varepsilon_2) + \bar{\tau}_c(\varepsilon_2).$$

Thus, if (49) holds, then $|\tau_i(t)| \leq \tau_{i,\max}$ for all $t \in [0, T_f]$ and all i . \square

Theorem 5 (Local wheel-momentum feasibility). *Assume Assumption 3 holds, i.e., $\|H(t)\| \leq H_{\max}$ on $[0, T_f]$, and the*

outer-loop reference is planned under the tightened wheel-momentum bound

$$|h_{w,d,i}(t)| \leq (1 - \gamma_h) h_{w,i,\max}, \quad \forall t \in [0, T_f], i = 1, 2, 3. \quad (59)$$

Assume further that the tracking errors satisfy

$$\|\sigma_e(t)\| \leq \varepsilon_1, \quad \|s(t)\| \leq \varepsilon_2, \quad \forall t \in [0, T_f]. \quad (60)$$

Let $\bar{Q} := \sup_{\|\sigma_e\| \leq \varepsilon_1} \|\mathbf{Q}(\sigma_e)\|$ and $\mu_i := \sum_{j=1}^3 |J_{ij}|$. If γ_h is chosen such that

$$H_{\max} + \mu_i (\omega_{d,\max} + \varepsilon_2 + \bar{Q}) \leq \gamma_h h_{w,i,\max}, \quad i = 1, 2, 3, \quad (61)$$

then the wheel momentum constraint holds for all $t \in [0, T_f]$:

$$|h_{w,i}(t)| \leq h_{w,i,\max}, \quad i = 1, 2, 3. \quad (62)$$

Proof. From $\mathbf{H} = \mathbf{J}\omega + \mathbf{h}_w$ we have $\mathbf{h}_w = \mathbf{H} - \mathbf{J}\omega$ and similarly $\mathbf{h}_{w,d} = \mathbf{H}_d - \mathbf{J}\omega_d$ for the reference. Subtracting yields

$$\mathbf{h}_w - \mathbf{h}_{w,d} = (\mathbf{H} - \mathbf{H}_d) - \mathbf{J}(\omega - \omega_d).$$

For the planner reference (disturbance-free), the total angular momentum is conserved; with $\mathbf{H}_d(0) = \mathbf{0}$, it follows that $\mathbf{H}_d(t) \equiv \mathbf{0}$ on $[0, T_f]$. Hence,

$$\mathbf{h}_w - \mathbf{h}_{w,d} = \mathbf{H} - \mathbf{J}\omega_e.$$

Therefore, for each axis i ,

$$|h_{w,i}| \leq |h_{w,d,i}| + |H_i| + |(\mathbf{J}\omega_e)_i|.$$

Using (59), $|H_i| \leq \|\mathbf{H}\| \leq H_{\max}$, and $|(\mathbf{J}\omega_e)_i| \leq \mu_i \|\omega_e\|$, we obtain

$$|h_{w,i}(t)| \leq (1 - \gamma_h) h_{w,i,\max} + H_{\max} + \mu_i \|\omega_e(t)\|.$$

Moreover, on the tube (60), $\omega_e = s - \mathbf{Q}(\sigma_e)$ gives $\|\omega_e\| \leq \|s\| + \|\mathbf{Q}\| \leq \varepsilon_2 + \bar{Q}$. In addition, $\|\omega_d(t)\| \leq \omega_{d,\max}$ implies $\|\omega(t)\| \leq \|\omega_d(t)\| + \|\omega_e(t)\| \leq \omega_{d,\max} + \varepsilon_2 + \bar{Q}$, so the envelope in (61) is valid. Consequently,

$$|h_{w,i}(t)| \leq (1 - \gamma_h) h_{w,i,\max} + H_{\max} + \mu_i (\omega_{d,\max} + \varepsilon_2 + \bar{Q}).$$

If (61) holds, then $|h_{w,i}(t)| \leq h_{w,i,\max}$ for all $t \in [0, T_f]$. \square

Remark 7. *The closed-loop system is initialized on the planned reference trajectory, i.e., $\sigma(0) = \sigma_d(0)$ and $\omega(0) = \omega_d(0)$, hence $\sigma_e(0) = \mathbf{0}$ and $s(0) = \mathbf{0}$. By Theorems 2–3, the regularized neighborhoods $\{\|s\| \leq \varepsilon_2\}$ and $\{\|\sigma_e\| \leq \varepsilon_1\}$ are forward invariant; once entered, the trajectories do not leave. Therefore, in this paper the condition in Theorem 4 and Theorem 5 holds over $[0, T_f]$.*

C. Overall Design Procedure of the TPA–PTC Framework

This subsection summarizes a mission-driven synthesis procedure for the proposed TPA–PTC framework.

- 1) **Mission inputs and physical limits.** Specify the terminal time $T_f > 0$ and the mission accuracy requirement $\varepsilon_{\text{mission}} > 0$. The inertia \mathbf{J} , wheel limits $\tau_{\max}, h_{w,\max}$, and disturbance bound d_{\max} (Assumption 2) are known.
- 2) **Margins and feasibility.** Choose tightening margins $\gamma_u, \gamma_h \in (0, 1)$ to reserve actuation headroom, e.g. $\gamma_u \gtrsim 2d_{\max}/u_{\max}$ (similarly for γ_h). Verify $T_f \geq T_{f,\min}$ (Assumption 1) via time-optimal analysis or a numerical feasibility test.
- 3) **Outer-loop planning** Solve the constrained OCP (25) on $[0, T_f]$ with tightened bounds $|\tau_i(t)| \leq (1 - \gamma_u)\tau_{i,\max}$ and $|h_{w,i}(t)| \leq (1 - \gamma_h)h_{w,i,\max}$. This produces a dynamically feasible reference trajectory $(\sigma_d, \omega_d, \dot{\omega}_d)$ that reaches the target exactly at $t = T_f$.
- 4) **Accuracy/time allocation and ε_2 scaling.** Set $\varepsilon_1 := \varepsilon_{\text{mission}}$, pick $\eta \in (0, 1)$, and allocate $T_{p1}, T_{p2} > 0$ such that $T_{p1} + T_{p2} < T_f$. Since the sliding surface is $s = \omega_e + \mathbf{Q}(\sigma_e)$ and $\|\mathbf{Q}\| = \mathcal{O}(\|\sigma_e\|^{1-\eta})$, set

$$\varepsilon_2 = c \varepsilon_1^{1-\eta}, \quad c > 0. \quad (63)$$

- 5) **Gain selection.** Choose $\alpha_1, \alpha_2 > 0$ such that $\varepsilon_{\delta_1} \leq \varepsilon_1$ and $\varepsilon_{\delta_2} \leq \varepsilon_2$ in Theorems 2–3. With $s_{\max} = \varepsilon_2$ and $\delta_2 = d_{\max} \sqrt{2/\lambda_{\min}(\mathbf{J})}$, sufficient lower bounds are

$$\alpha_1 \geq \alpha_{1,\min} := \frac{\eta T_{p1}}{\pi} 2^{-\eta/2} \frac{\varepsilon_2}{\varepsilon_1^{1-\eta}}, \quad \alpha_2 \geq \alpha_{2,\min} := \frac{\delta_2 \eta T_{p2}}{\pi} \left(\frac{\sqrt{2}}{\varepsilon_2} \right)^{1-\eta}. \quad (64)$$

- 6) **Verify saturation feasibility.** Using the planned reference and the resulting ε_σ from Step 3, verify the sufficient non-saturation condition in Theorem 4. If violated, increase T_f (or T_{p1}, T_{p2}), relax ε_1 , or replan with larger margins γ_u, γ_h and/or a smoother reference.

It is worth noting that the proposed synthesis is not tuning-intensive. In practice, the only parameter that typically requires adjustment is the exponent η , which mainly trades off smoothness and transient aggressiveness. The remaining quantities are either specified by the mission and hardware ($T_f, \varepsilon_{\text{mission}}, u_{\max}, h_{w,\max}, d_{\max}, \mathbf{J}$) or chosen as conservative robustness margins ($\gamma_u, \gamma_h, \kappa$). Once these are set, the rest of the controller parameters (including ε_2 and α_1, α_2) follow

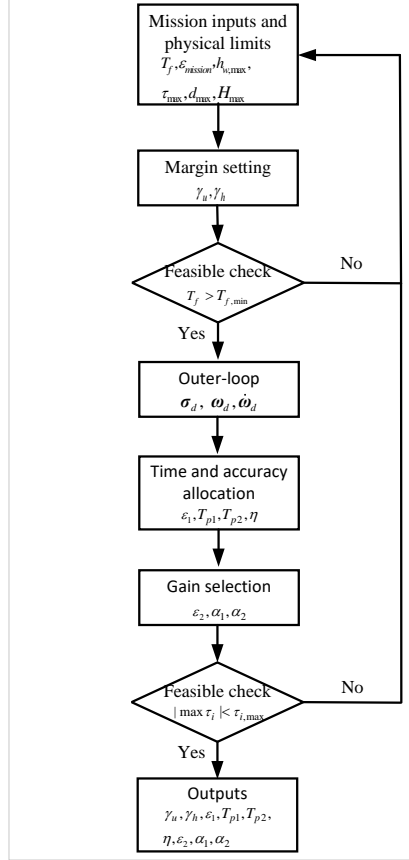


Fig. 2 overall design procedure of the TPA–PTC framework.

automatically from the closed-form rules above.

Remark 8 (Recommended balanced synthesis). *While (63) provides a physically meaningful scaling between ε_2 and ε_1 , the constant c may be selected automatically to avoid unbalanced gains. A convenient choice is to enforce $\alpha_1 = \alpha_2 = \kappa \alpha$ with a safety factor $\kappa > 1$, and determine ε_2 and α by solving $\alpha_{1,\min} = \alpha_{2,\min}$ in (64). This yields*

$$\varepsilon_2 = \left(\frac{\delta_2 \eta T_{p2}}{\eta T_{p1}} 2^{1/2} \right)^{\frac{1}{2-\eta}} \varepsilon_1^{\frac{1-\eta}{2-\eta}}, \quad \alpha = \frac{\eta T_{p1}}{\pi} 2^{-\eta/2} \frac{\varepsilon_2}{\varepsilon_1^{1-\eta}}, \quad (65)$$

followed by $\alpha_1 = \alpha_2 = \kappa \alpha$. This balanced rule yields a unique and reproducible parameter set from mission inputs and physical limits.

IV. Simulation Results

Numerical simulations are conducted to validate the proposed TPA–PTC framework under dual reaction-wheel saturation. Table 2 summarizes the common spacecraft parameters, actuator limits, disturbance model, and maneuver boundary conditions used throughout this section. The theoretical results are established on the mission interval $[0, T_f]$;

for visualization of the post-maneuver behavior, the simulation horizon is extended to $T_{\text{sim}} > T_f$. For $t \geq T_f$, the reference is held constant at the target state, i.e., $\sigma_d(t) = \sigma_{\text{target}}$ and $\omega_d(t) = \omega_{\text{target}}$.

Table 2 Common simulation settings and boundary conditions

Symbol	Value
J	$\text{diag}([200, 250, 300]) \text{ kg} \cdot \text{m}^2$
$\tau_{i,\text{max}}$	$0.2 \text{ N} \cdot \text{m}$
$h_{w,i,\text{max}}$	$4.0 \text{ kg} \cdot \text{m}^2/\text{s}$
$d(t)$	$0.01 [\sin(2t), \cos(t), \cos(t+2)]^\top \text{ N} \cdot \text{m}$
d_{max}	$\sqrt{3} \times 0.01 \text{ N} \cdot \text{m}$
$\sigma(0)$	$[0.2, 0.3, -0.3]^\top$
σ_{target}	$[0, 0, 0]^\top$
$\omega(0)$	$[0, 0, 0]^\top \text{ rad/s}$
ω_{target}	$[0, 0, 0]^\top \text{ rad/s}$
$h_w(0)$	$[0, 0, 0]^\top \text{ kg} \cdot \text{m}^2/\text{s}$

The outer-loop reference (σ_d, ω_d) is generated offline by solving the constrained OCP (25) using GPOPS-II with $\lambda = 0.1$ and $N = 20$ nodes. The nodal torques are converted to a continuous-time command via piecewise-linear interpolation (26).

Four scenarios are reported in this section: Case 1 presents a baseline timed maneuver to verify tracking performance and dual-constraint compliance; Case 2 sweeps the commanded terminal time T_f to assess time anchoring and actuation usage; Case 3 sweeps the prescribed accuracy ε_1 to demonstrate accuracy tunability and the associated control effort; and Case 4 compares against a conventional prescribed-time controller under enforced saturation.

A. Case 1: Baseline Maneuver

This case validates the baseline performance of the proposed TPA–PTC framework, including time-anchored arrival at the commanded terminal instant and strict compliance with the dual actuator constraints. The commanded terminal time and mission-level attitude accuracy are set to $T_f = 120 \text{ s}$ and $\varepsilon_1 = \varepsilon_{\text{mission}} = 10^{-5}$, respectively. We allocate the inner-loop convergence times as $T_{p2} = 15 \text{ s}$ and $T_{p1} = 100 \text{ s}$, so that $T_{p1} + T_{p2} = 115 \text{ s} < T_f$. The exponent is set to $\eta = 0.2$, and the tightening margins are chosen as $\gamma_u = \gamma_h = 0.1$.

Following the synthesis procedure in Section III.C with $\kappa = 1.2$, the remaining inner-loop parameters are obtained as $\varepsilon_2 = 8.0213 \times 10^{-5}$ and $\alpha_1 = \alpha_2 = 5.7174$. The practical convergence bounds predicted by Theorems 2–3 are $\varepsilon_{\delta_1} = 7.9620 \times 10^{-6}$ and $\varepsilon_{\delta_2} = 6.3865 \times 10^{-5}$, which satisfy $\varepsilon_{\delta_1} < \varepsilon_1$ and $\varepsilon_{\delta_2} < \varepsilon_2$. Therefore, the ultimate neighborhoods are governed by the user-selected tolerances $(\varepsilon_1, \varepsilon_2)$.

With the above parameter set, the closed-loop responses are shown in Figs. 3–5. Figure 3 indicates that the spacecraft tracks the planned reference closely in both MRPs and angular velocity. Since the outer-loop reference satisfies the

terminal boundary conditions at $t = T_f$ by construction, the actual state reaches the target at the commanded terminal instant with the prescribed tracking accuracy.

The error responses are summarized in Fig. 4. Because the maneuver is initialized consistently with the planned reference ($\sigma(0) = \sigma_d(0)$ and $\omega(0) = \omega_d(0)$), the tracking errors start at $\sigma_e(0) = \mathbf{0}$ and $\omega_e(0) = \mathbf{0}$, and thus $s(0) = \mathbf{0}$ as well. Accordingly, all three errors remain near the origin throughout the maneuver and stay within their prescribed neighborhoods, while the reference continues to evolve until T_f , thereby preserving time anchoring.

Figure 5 verifies physical realizability under dual saturation: all torque components satisfy $|\tau_i(t)| \leq \tau_{i,\max}$ and the wheel momentum satisfies $|h_{w,i}(t)| \leq h_{w,i,\max}$ for all axes over the entire interval $t \in [0, T_f]$.

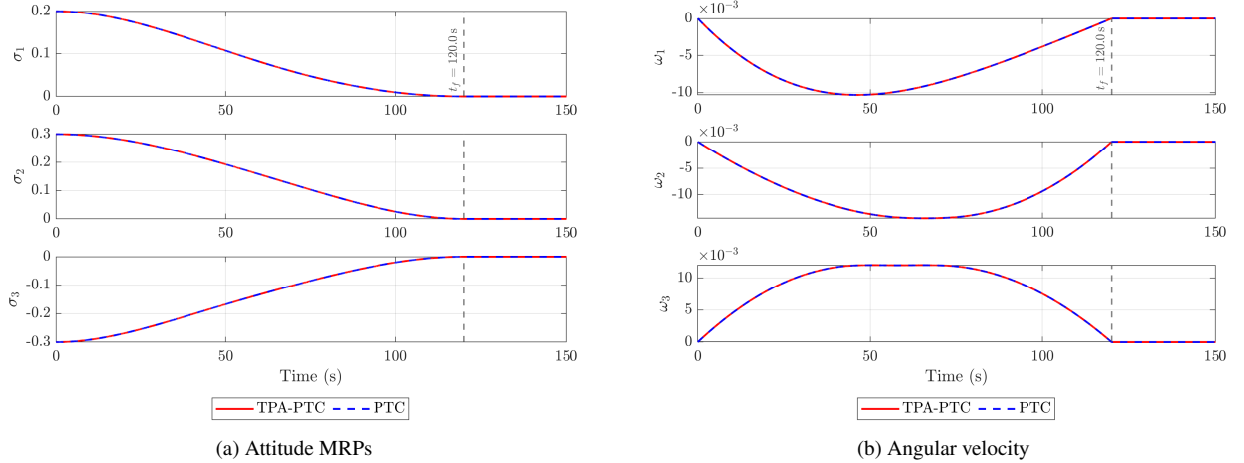


Fig. 3 Case 1: Reference tracking in MRPs and angular rates.

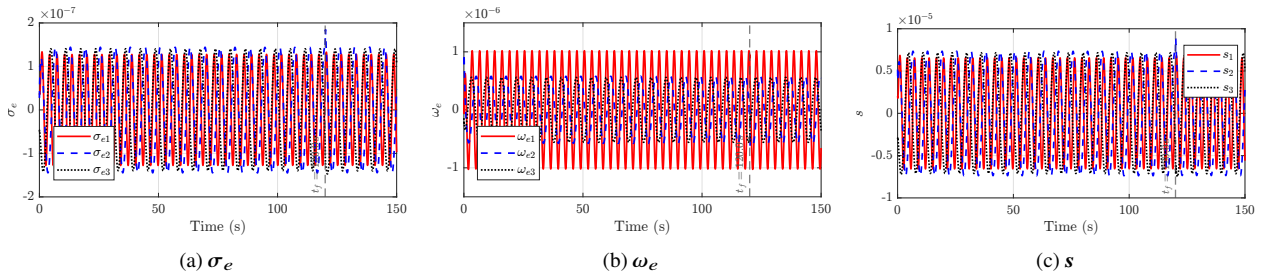


Fig. 4 Case 1: Errors responses

To assess robustness against a beyond-bound transient perturbation, we apply a strong disturbance during the first second:

$$\mathbf{d}(t) = \begin{cases} 0.05 [1, 1, 1]^\top \text{ N} \cdot \text{m}, & 0 \leq t < 1, \\ \mathbf{d}_{\text{base}}(t), & t \geq 1, \end{cases} \quad (66)$$

where $\mathbf{d}_{\text{base}}(t)$ is the bounded disturbance in Table 2. Since $0.05 \text{ N} \cdot \text{m} > d_{\max}$, this injection can drive the trajectory temporarily outside the practical convergence neighborhoods guaranteed under Assumption 2. Nevertheless, Figs. 6–7

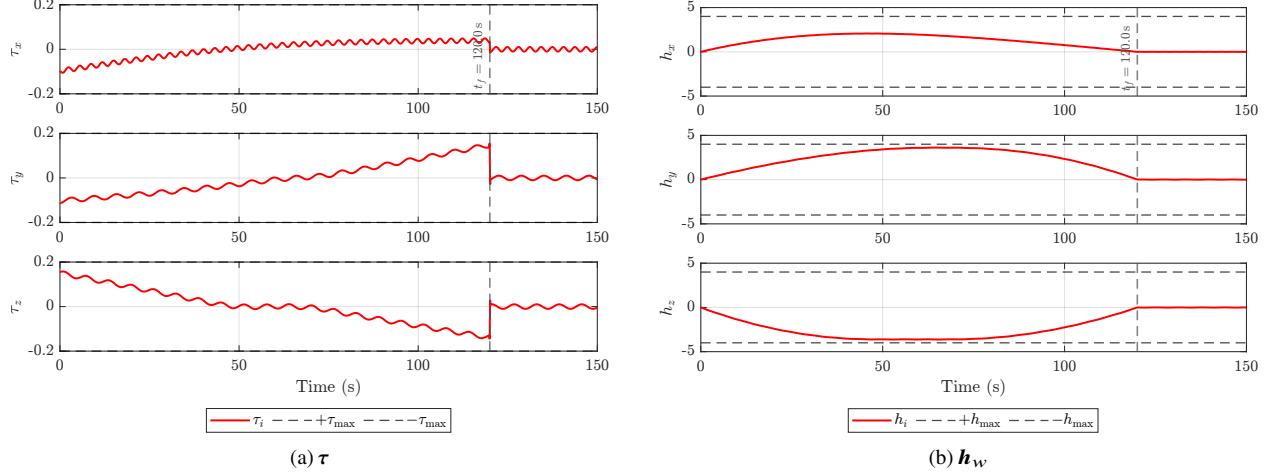


Fig. 5 Case 1: Torque and wheel momentum.

show that once the transient is removed at $t = 1$ s, the tracking errors rapidly return to their prescribed neighborhoods within the scheduled time $T_{p1} + T_{p2}$, while the torque and wheel momentum remain within their limits throughout the maneuver.

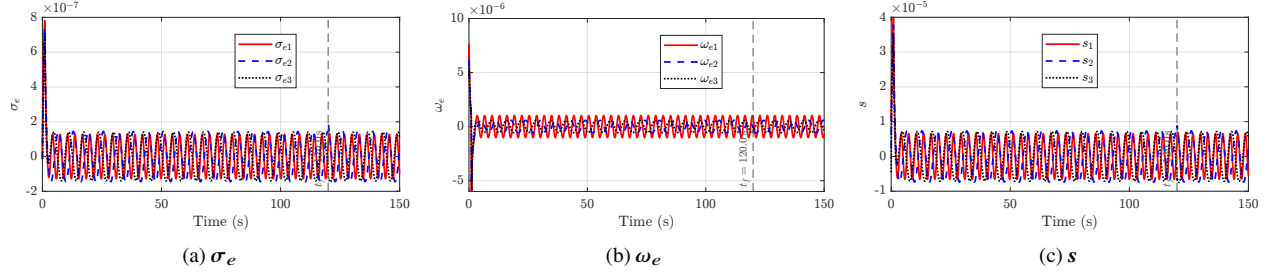


Fig. 6 Case 1: Errors under the beyond-bound transient disturbance.

Overall, this case demonstrates time-anchored terminal convergence with dual-constraint compliance, and confirms recovery into the prescribed neighborhoods within $T_{p1} + T_{p2}$ even under a beyond-bound transient perturbation.

B. Case 2: Time-Flexibility Assessment

Before presenting Case 2, we clarify the error notation used in the plots. The tracking error σ_e in Sections II–III is defined with respect to the reference $\sigma_d(t)$. In this case, to visualize time anchoring relative to the fixed terminal command, we additionally report the target-pointing MRP error $\sigma_{e,\text{tar}}$, defined between the current attitude $\sigma(t)$ and the constant target attitude σ_{target} via the same MRP error mapping.

This case verifies that the proposed framework preserves time anchoring across different commanded terminal times while remaining feasible under dual actuator constraints. For all $T_f \in \{110\text{ s}, 120\text{ s}, 130\text{ s}, 140\text{ s}\}$, the closed-loop system reaches the target at the commanded terminal instant with the prescribed tracking accuracy, and both the control torque and wheel momentum remain within their limits.

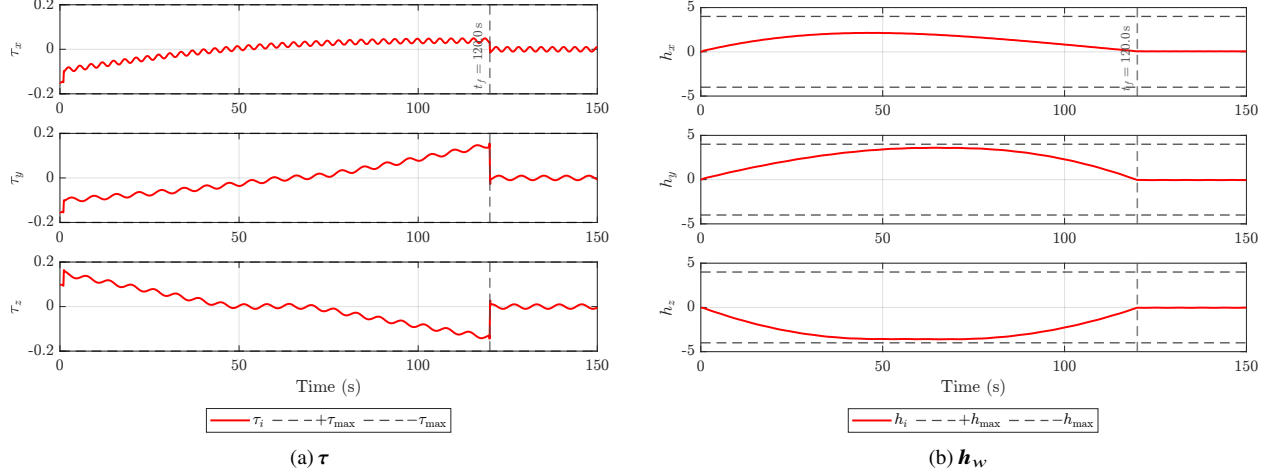


Fig. 7 Case 1: Torque and wheel momentum under the beyond-bound transient disturbance.

The study is conducted under the same settings in Table 2, with $\varepsilon_1 = 10^{-5}$, $\eta = 0.2$, $\gamma_u = \gamma_h = 0.1$, and the time allocation $T_{p2} = 15$ s, $T_{p1} = T_f - 20$ s (so $T_{p1} + T_{p2} = T_f - 5$ s < T_f). For each commanded T_f , the outer-loop OCP (25) is solved on $[0, T_f]$ to generate a dual-constraint-feasible reference, and the remaining inner-loop parameters ($\varepsilon_2, \alpha_1, \alpha_2$) are synthesized by the balanced rule in Section III.C with $\kappa = 1.2$; the resulting values are listed in Table 3.

Table 3 Case 2: Synthesized parameters for terminal-time sweep

T_f	T_{p1}	T_{p2}	ε_2	$\alpha_1 = \alpha_2$
110 s	90 s	15 s	8.505×10^{-5}	5.456
120 s	100 s	15 s	8.021×10^{-5}	5.717
130 s	110 s	15 s	7.608×10^{-5}	5.965
140 s	120 s	15 s	7.249×10^{-5}	6.200

Figures 8–10 summarize the responses. Figure 8 shows that the target-pointing error components $\sigma_{e,\text{tar}}$ decay into small neighborhoods before their respective terminal instants, demonstrating the commanded time anchoring. Figures 9 and 10 further reveal the expected trade-off: shorter T_f requires more aggressive actuation, resulting in higher torque demand and faster wheel-momentum accumulation, yet both remain within the hardware limits due to the dual-constraint-aware planning and bounded inner-loop corrections.

In summary, Case 2 confirms that the proposed framework provides a practical interface to schedule the maneuver at user-specified terminal times. By re-planning the dual-constraint-feasible reference on $[0, T_f]$ and re-synthesizing the tracking parameters accordingly, the closed-loop system preserves time anchoring across a wide range of T_f values. The results also reveal the expected trade-off: shorter T_f leads to higher torque demand and faster wheel-momentum accumulation, while all runs remain realizable under the prescribed actuator limits due to the constraint-aware co-design.

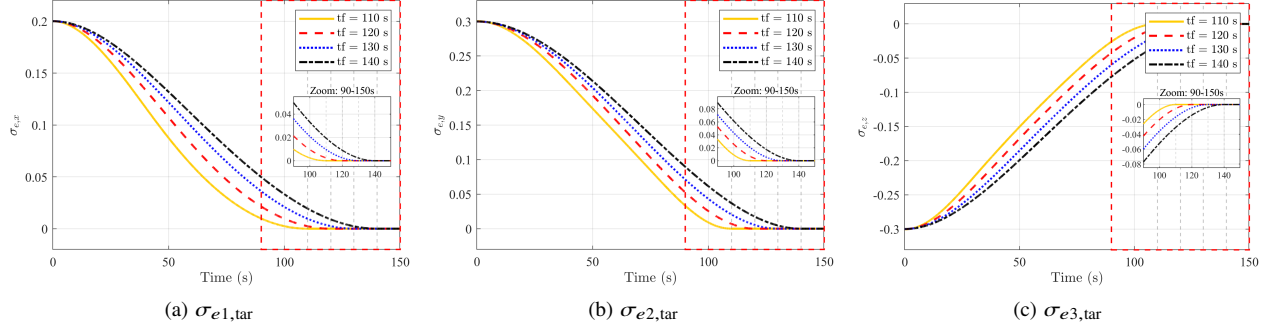


Fig. 8 Case 2: MRP error components for different T_f

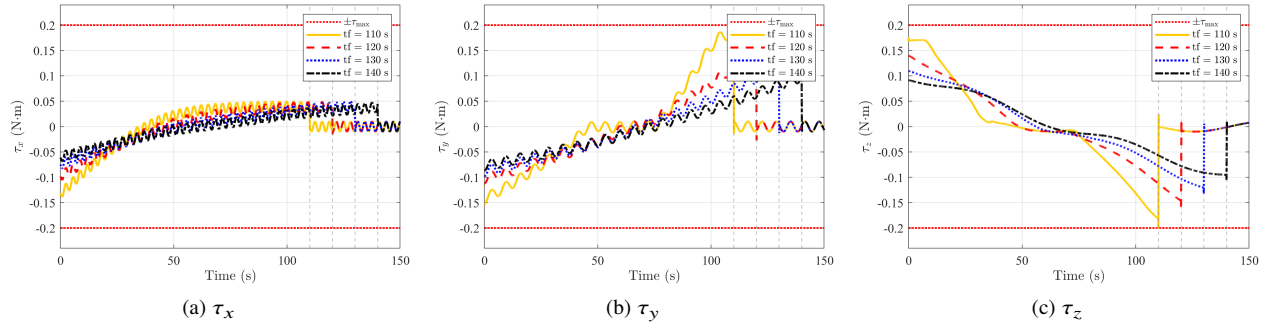


Fig. 9 Case 2: Control torque components for different T_f

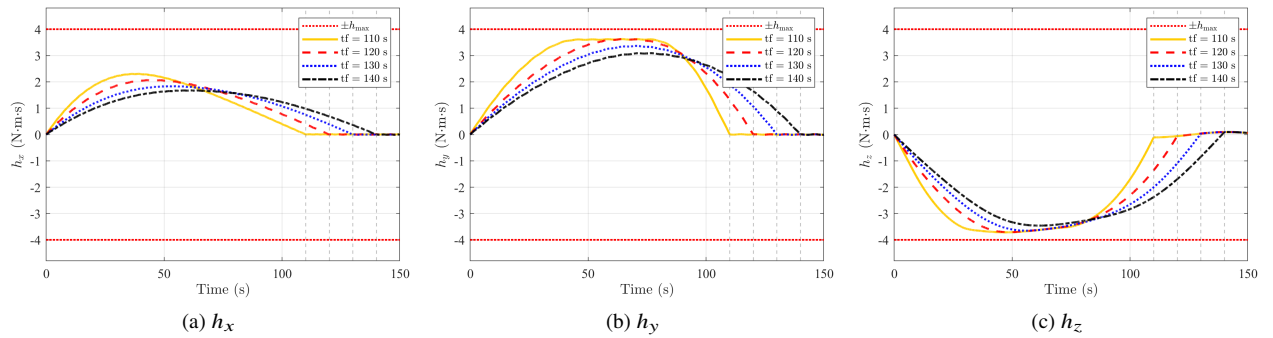


Fig. 10 Case 2: Wheel momentum components for different T_f

C. Case 3: Precision-sweep assessment under identical conditions

This case demonstrates prescribed-accuracy tunability under the same operating condition as Case 1, with the terminal time fixed at $T_f = 120$ s. Set $\eta = 0.2$, $\gamma_u = \gamma_h = 0.1$, $T_{p2} = 15$ s, and $T_{p1} = 100$ s, and sweep the prescribed attitude tolerance as $\varepsilon_1 \in \{10^{-4}, 10^{-5}, 10^{-6}, 10^{-7}\}$. For each ε_1 , the remaining inner-loop parameters are synthesized using the balanced rule in Section III.C with $\kappa = 1.2$, producing $(\varepsilon_2, \alpha_1, \alpha_2)$ together with the practical bounds $(\varepsilon_{\delta_1}, \varepsilon_{\delta_2})$ from Theorems 2–3. The resulting values are reported in Table 4.

Table 4 Case 3: Synthesized parameters for accuracy sweep

ε_1	ε_2	$\alpha_1 = \alpha_2$	ε_{δ_1}	ε_{δ_2}
1×10^{-4}	2.232×10^{-4}	2.521	7.962×10^{-5}	1.777×10^{-4}
1×10^{-5}	8.021×10^{-5}	5.717	7.962×10^{-6}	6.387×10^{-5}
1×10^{-6}	2.883×10^{-5}	12.965	7.962×10^{-7}	2.295×10^{-5}
1×10^{-7}	1.036×10^{-5}	29.398	7.962×10^{-8}	8.249×10^{-6}

The log-scale responses are compared in Fig. 11. Figure 11 shows that all four runs meet their prescribed accuracy requirements: $\|\sigma_e(t)\|$ decreases below the corresponding threshold ε_1 and remains within that neighborhood thereafter, while $\|s(t)\|$ is regulated below its synthesized bound ε_2 . This confirms that the proposed framework provides a direct and reliable interface for tuning mission accuracy through ε_1 under the same terminal-time specification.

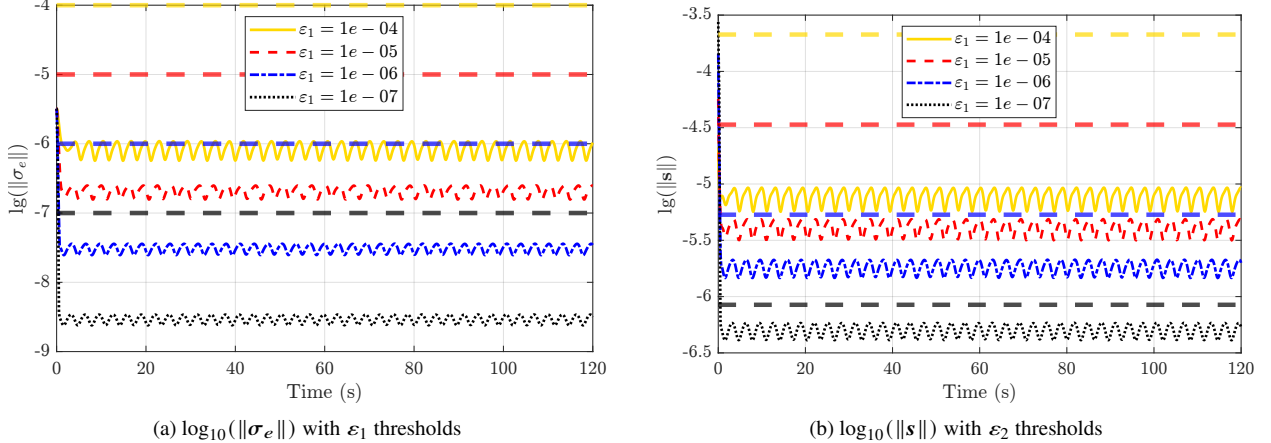


Fig. 11 Case 3: Log-scale comparison of $\|\sigma_e\|$ and $\|s\|$ for different ε_1

As ε_1 is tightened from 10^{-4} to 10^{-7} , the achieved steady-state tracking level decreases accordingly, and the induced sliding tolerance ε_2 also decreases. Meanwhile, the synthesis rules increases the gains α_1 and α_2 substantially (Table 4), which leads to higher control activity and reduced robustness margins. Therefore, in practical implementations ε_1 should be selected according to sensor/estimation capability and available actuation resources; pursuing excessively small numerical tolerances is unnecessary and may degrade robustness.

In summary, Case 3 confirms that the proposed framework can systematically enforce different prescribed accuracy

levels through ε_1 under the same terminal-time specification. Tightening ε_1 reduces the tracking residual as expected, but it requires significantly larger synthesized gains and thus higher control activity. Therefore, ε_1 should be selected to match achievable sensing/estimation accuracy and available actuation margins, rather than pursuing overly small numerical tolerances.

D. Case 4: Comparison with PTC under actuator saturation

This case compares the proposed TPA-PTC with the predefined-time controller in [10], both commanded with $T_f = 120$ s under the same initial condition and disturbance. The controller in [10] is derived under unconstrained actuation (no explicit torque or wheel-momentum limits). In our implementation, its nominal predefined-time convergence is reproduced when saturation is inactive (i.e., when the limits are set sufficiently large so that the commanded torque is not clipped). Then enforce practical actuator limits and examine how saturation affects its terminal-time performance. Two saturation settings are considered: (i) torque saturation only, and (ii) dual saturation (torque and wheel momentum). The key metric is the terminal pointing error at $t = T_f$, while the settling behavior is reported as a supplement.

1. Case 4.1: Torque saturation only

Figure 12 compares the tracking errors, angular-rate errors and the control torque under torque saturation. With saturation, the baseline controller exhibits overshoots and non-monotonic error transients, and the error does not reach the desired neighborhood by the commanded terminal time; the observed settling is around 160 s in this setup. In contrast, TPA-PTC reaches the target at $t = T_f$ while keeping the torque within bounds, enabled by the torque-feasible reference planning and bounded tracking corrections.

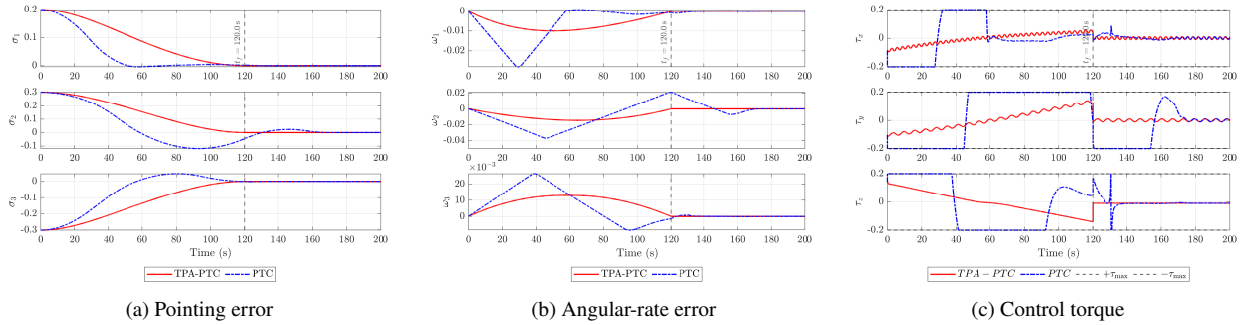


Fig. 12 Case 4.1: Comparison under torque saturation

2. Case 4.2: Dual saturation (torque and wheel momentum)

Figure 13 shows the comparison when dual saturation are enforced. Dual saturation further reduces the effective control authority, leading to larger overshoots and prolonged near-saturation operation for the baseline controller; the

settling time increases substantially (about 350 s in this setup), and the terminal error at $t = T_f$ remains large. In contrast, TPA–PTC preserves time anchoring and feasibility under dual saturation by planning a dual-constraint-feasible reference on $[0, T_f]$ and tracking it with a nonsingular prescribed-time law with bounded corrections.

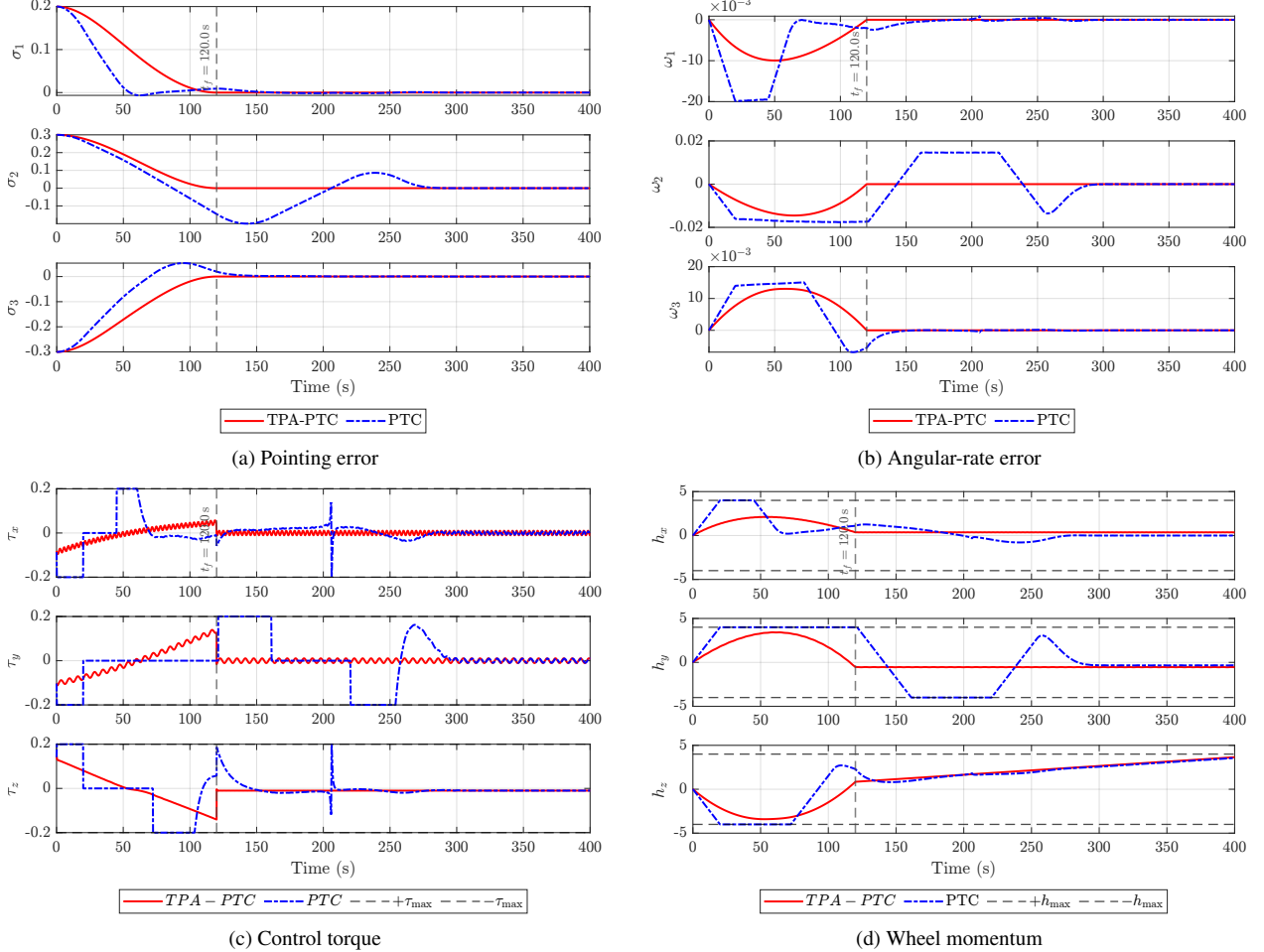


Fig. 13 Case 4.2: Comparison under dual saturation

In summary, Case 4 shows that enforcing actuator saturation can destroy the nominal terminal-time behavior of predefined-time controllers derived under unconstrained assumptions, whereas TPA–PTC maintains time anchoring by co-designing a saturation-feasible reference and a bounded prescribed-time tracker.

V. Conclusion

This paper proposed a Timed Prescribed-Accuracy and Prescribed-Time Control (TPA–PTC) framework for reaction-wheel spacecraft that must reach a commanded attitude *exactly* at a user-specified terminal time while strictly satisfying both torque and wheel momentum limits. The approach combines a constraint-aware, time-anchored trajectory planner with a nonsingular prescribed-time tracking controller, yielding explicit practical prescribed-time accuracy

bounds and a sufficient feasibility condition that relates actuator limits, margins, prescribed-time parameters, and admissible initial errors.

Simulation results demonstrated exact-time arrival with guaranteed constraint satisfaction under significant disturbances, consistent performance across multiple prescribed terminal times, and predictable accuracy changes under a precision sweep. Comparisons with a conventional prescribed-time controller under enforced actuator constraints further illustrated that saturation can destroy the nominal prescribed-time behavior and significantly prolong settling, underscoring the necessity of constraint-aware co-design for physically realizable timed maneuvers.

Future work will investigate reduced-complexity/online planning, robustness to model uncertainty, and integrated momentum-management strategies for long-duration operations.

A. A Bang-Bang Estimate of $T_{f,\min}$

This appendix provides a bang-bang estimate of the minimum feasible maneuver time under component-wise torque and wheel-momentum limits. It is used as a conservative screening rule for selecting T_f in Assumption 1.

Let $\sigma_e(0)$ denote the initial attitude error in MRPs. The associated principal rotation angle $\theta \in [0, \pi]$ and axis $\mathbf{e} = [e_1, e_2, e_3]^T$ are

$$\theta = 4 \arctan(\|\sigma_e(0)\|), \quad \mathbf{e} = \begin{cases} \frac{\sigma_e(0)}{\|\sigma_e(0)\|}, & \sigma_e(0) \neq \mathbf{0}, \\ \text{any unit vector,} & \sigma_e(0) = \mathbf{0}. \end{cases} \quad (67)$$

Define the effective inertia $J_e := \mathbf{e}^T \mathbf{J} \mathbf{e}$. With $|\tau_i| \leq \tau_{i,\max}$, the maximum torque projection along \mathbf{e} is

$$\tau_{e,\max} = \max_{|\tau_i| \leq \tau_{i,\max}} \mathbf{e}^T \boldsymbol{\tau} = \sum_{i=1}^3 |e_i| \tau_{i,\max}. \quad (68)$$

Assume $\mathbf{h}_w(0) = \mathbf{0}$ and $|h_{w,i}| \leq h_{w,i,\max}$. Under the bang-bang allocation $\tau_i = \text{sgn}(e_i) \tau_{i,\max}$, the maximum duration before wheel-momentum saturation is

$$t_h := \min_{i \in \{1,2,3\}} \frac{h_{w,i,\max}}{\tau_{i,\max}}. \quad (69)$$

For a nominal rest-to-rest rotation about \mathbf{e} , the peak rate and the corresponding no-coast angle are

$$\omega_{\max} = \frac{\tau_{e,\max}}{J_e} t_h, \quad \theta_h = \frac{\tau_{e,\max}}{J_e} t_h^2. \quad (70)$$

The resulting minimum-time estimate is

$$T_{f,\min} \approx \begin{cases} 2\sqrt{\frac{J_e \theta}{\tau_{e,\max}}}, & \theta \leq \theta_h, \\ 2t_h + \frac{\theta - \theta_h}{\omega_{\max}}, & \theta > \theta_h. \end{cases} \quad (71)$$

B. Bound on the feedforward mismatch

Define the total angular momentum (body frame) as

$$\mathbf{H}(t) := \mathbf{J}\boldsymbol{\omega}(t) + \mathbf{h}_w(t), \quad \mathbf{H}_d(t) := \mathbf{J}\boldsymbol{\omega}_d(t) + \mathbf{h}_{w,d}(t). \quad (72)$$

The planned torque associated with the outer-loop reference is

$$\boldsymbol{\tau}_{\text{ref}}(t) = \mathbf{J}\dot{\boldsymbol{\omega}}_d(t) + \boldsymbol{\omega}_d(t)^{\times}\mathbf{H}_d(t), \quad (73)$$

and the feedforward mismatch is defined by

$$\Delta_f(t) := \mathbf{f}(t) - \boldsymbol{\tau}_{\text{ref}}(t). \quad (74)$$

Substituting $\mathbf{f}(t)$ from (9) yields

$$\Delta_f(t) = -\boldsymbol{\omega}(t)^{\times}\mathbf{H}(t) + \mathbf{J}\boldsymbol{\omega}_e(t)^{\times}\mathbf{R}(\boldsymbol{\sigma}_e(t))\boldsymbol{\omega}_d(t) + \mathbf{J}(\mathbf{R}(\boldsymbol{\sigma}_e(t)) - \mathbf{I})\dot{\boldsymbol{\omega}}_d(t) - \boldsymbol{\omega}_d(t)^{\times}\mathbf{H}_d(t). \quad (75)$$

The outer-loop reference is generated under wheel-only actuation and disturbance-free dynamics. Moreover, Assumption 3 enforces a zero reference total angular momentum, i.e., $\mathbf{H}_d(t) \equiv \mathbf{0}$. Hence, the last term in (75) vanishes and $\boldsymbol{\tau}_{\text{ref}}(t) = \mathbf{J}\dot{\boldsymbol{\omega}}_d(t)$.

For the attitude-dependent term, using (7) one has

$$\|\mathbf{R}(\boldsymbol{\sigma}_e) - \mathbf{I}\| = \frac{4\|\boldsymbol{\sigma}_e\|}{1 + \|\boldsymbol{\sigma}_e\|^2} \leq 4\|\boldsymbol{\sigma}_e\|. \quad (76)$$

Let $\mu_i := \sum_{j=1}^3 |J_{ij}|$ so that $|(\mathbf{J}\mathbf{v})_i| \leq \mu_i \|\mathbf{v}\|_2$. Using $\|\mathbf{a}^{\times}\mathbf{b}\| \leq \|\mathbf{a}\| \|\mathbf{b}\|$, $\|\mathbf{R}\| = 1$, and the mission-level momentum budget $\|\mathbf{H}(t)\| \leq H_{\max}$ from Assumption 3, we obtain for each axis i :

$$|\Delta_{f,i}(t)| \leq \|\boldsymbol{\omega}(t)\| H_{\max} + \mu_i \|\boldsymbol{\omega}_e(t)\| \|\boldsymbol{\omega}_d(t)\| + 4\mu_i \|\boldsymbol{\sigma}_e(t)\| \|\dot{\boldsymbol{\omega}}_d(t)\|. \quad (77)$$

Furthermore, since $\|\omega(t)\| \leq \|\omega_e(t)\| + \|\omega_d(t)\|$, it follows that

$$|\Delta_{f,i}(t)| \leq (\|\omega_e(t)\| + \|\omega_d(t)\|) H_{\max} + \mu_i \|\omega_e(t)\| \|\omega_d(t)\| + 4\mu_i \|\sigma_e(t)\| \|\dot{\omega}_d(t)\|. \quad (78)$$

Taking the supremum on $[0, T_f]$, for any valid bounds $\|\omega_e(t)\| \leq \omega_{e,\max}$, $\|\sigma_e(t)\| \leq \sigma_{\max}$, $\|\omega_d(t)\| \leq \omega_{d,\max}$, $\|\dot{\omega}_d(t)\| \leq \dot{\omega}_{d,\max}$, one may choose the component-wise envelope

$$\Delta_{f,i,\max} := (\omega_{e,\max} + \omega_{d,\max}) H_{\max} + \mu_i \omega_{e,\max} \omega_{d,\max} + 4\mu_i \sigma_{\max} \dot{\omega}_{d,\max}, \quad i = 1, 2, 3. \quad (79)$$

References

- [1] Alex Pothen, A., Crain, A., and Ulrich, S., “Pose Tracking Control for Spacecraft Proximity Operations Using the Udwadia–Kalaba Framework,” *Journal of Guidance, Control, and Dynamics*, Vol. 45, No. 2, 2022, pp. 296–309. <https://doi.org/10.2514/1.G005169>, URL <https://doi.org/10.2514/1.G005169>, publisher: American Institute of Aeronautics and Astronautics _eprint: <https://doi.org/10.2514/1.G005169>.
- [2] Sun, H.-J., Wu, Y.-Y., and Zhang, J., “Attitude synchronization control for multiple spacecraft: A preassigned finite-time scheme,” *Advances in Space Research*, Vol. 73, No. 12, 2024, pp. 6094–6110. <https://doi.org/10.1016/j.asr.2024.02.001>, URL <https://www.sciencedirect.com/science/article/pii/S0273117724001303>.
- [3] Xu, C., Zelazo, D., and Wu, B., “Distributed prescribed-time coordinated control of spacecraft formation flying under input saturation,” *Advances in Space Research*, Vol. 74, No. 5, 2024, pp. 2302–2315. <https://doi.org/10.1016/j.asr.2024.05.077>, URL <https://www.sciencedirect.com/science/article/pii/S027311772400543X>.
- [4] Hong, Y., and Jiang, Z.-P., “Finite-Time Stabilization of Nonlinear Systems With Parametric and Dynamic Uncertainties,” *IEEE Transactions on Automatic Control*, Vol. 51, No. 12, 2006, pp. 1950–1956. <https://doi.org/10.1109/TAC.2006.886515>, URL <https://ieeexplore.ieee.org/document/4026648/>.
- [5] Polyakov, A., “Nonlinear Feedback Design for Fixed-Time Stabilization of Linear Control Systems,” *IEEE Transactions on Automatic Control*, Vol. 57, No. 8, 2012, pp. 2106–2110. <https://doi.org/10.1109/TAC.2011.2179869>, URL <https://ieeexplore.ieee.org/document/6104367/>.
- [6] Polyakov, A., Efimov, D., and Perruquetti, W., “Finite-time and fixed-time stabilization: Implicit Lyapunov function approach,” *Automatica*, Vol. 51, 2015, pp. 332–340. <https://doi.org/10.1016/j.automatica.2014.10.082>, URL <https://www.sciencedirect.com/science/article/pii/S0005109814004634>.
- [7] Sánchez-Torres, J. D., Sanchez, E. N., and Loukianov, A. G., “Predefined-time stability of dynamical systems with sliding modes,” *2015 American Control Conference (ACC)*, 2015, pp. 5842–5846. <https://doi.org/10.1109/ACC.2015.7172255>, URL <https://ieeexplore.ieee.org/document/7172255>, iSSN: 2378-5861.
- [8] Sánchez-Torres, J. D., Gómez-Gutiérrez, D., López, E., and Loukianov, A. G., “A class of predefined-time stable dynamical systems,” *IMA Journal of Mathematical Control and Information*, Vol. 35, No. Supplement_1, 2018, pp. i1–i29. <https://doi.org/10.1093/imamci/dnx004>, URL <https://doi.org/10.1093/imamci/dnx004>.
- [9] Anguiano-Gijón, C. A., Muñoz-Vázquez, A. J., Sánchez-Torres, J. D., Romero-Galván, G., and Martínez-Reyes, F., “On predefined-time synchronisation of chaotic systems,” *Chaos, Solitons & Fractals*, Vol. 122, 2019, pp. 172–178. <https://doi.org/10.1016/j.chaos.2019.03.015>, URL <https://www.sciencedirect.com/science/article/pii/S0960077919300864>.
- [10] Ye, D., Zou, A.-M., and Sun, Z., “Predefined-Time Predefined-Bounded Attitude Tracking Control for Rigid Spacecraft,” *IEEE Transactions on Aerospace and Electronic Systems*, Vol. 58, No. 1, 2022, pp. 464–472. <https://doi.org/10.1109/TAES.2021.3103258>, URL <https://ieeexplore.ieee.org/abstract/document/9512481>.

- [11] Muñoz-Vázquez, A. J., Sánchez-Torres, J. D., Gutiérrez-Alcalá, S., Jiménez-Rodríguez, E., and Loukianov, A. G., “Predefined-time robust contour tracking of robotic manipulators,” *Journal of the Franklin Institute*, Vol. 356, No. 5, 2019, pp. 2709–2722. <https://doi.org/10.1016/j.jfranklin.2019.01.041>, URL <https://www.sciencedirect.com/science/article/pii/S0016003219300973>.
- [12] Meng, Y., Zhu, Y., Cui, Y., and Qiao, J., “Predefined-Time Enhanced Antidisturbance Attitude Control for Rigid-Liquid Coupled Launch Vehicles,” *Journal of Guidance Control and Dynamics*, Vol. 48, No. 4, 2025, pp. 870–884. <https://doi.org/10.2514/1.G008397>, num Pages: 15 Place: Reston Publisher: Amer Inst Aeronautics Astronautics Web of Science ID: WOS:001403479000001.
- [13] Xiao, Y., Wang, Y., Ye, D., and Sun, Z., “Predefined-time robust attitude tracking control of flexible spacecraft with continuous and nonsingular performance,” *Aerospace Science and Technology*, Vol. 159, 2025, p. 110000. <https://doi.org/10.1016/j.ast.2025.110000>, URL <https://www.sciencedirect.com/science/article/pii/S1270963825000720>.
- [14] Xu, C., Wu, B., and Wang, D., “Distributed Prescribed-Time Attitude Coordination for Multiple Spacecraft With Actuator Saturation Under Directed Graph,” *IEEE Transactions on Aerospace and Electronic Systems*, Vol. 58, No. 4, 2022, pp. 2660–2672. <https://doi.org/10.1109/TAES.2021.3135484>, URL <https://ieeexplore.ieee.org/document/9650527/>.
- [15] Song, Y., Wang, Y., Holloway, J., and Krstic, M., “Time-varying feedback for regulation of normal-form nonlinear systems in prescribed finite time,” *AUTOMATICA*, Vol. 83, 2017, pp. 243–251. <https://doi.org/10.1016/j.automatica.2017.06.008>, URL <https://linkinghub.elsevier.com/retrieve/pii/S000510981730290X>, num Pages: 9 Place: Oxford Publisher: Pergamon-Elsevier Science Ltd Web of Science ID: WOS:000408288800028.
- [16] Zhou, B., “Finite-time stability analysis and stabilization by bounded linear time-varying feedback,” *Automatica*, Vol. 121, 2020, p. 109191. <https://doi.org/10.1016/j.automatica.2020.109191>, URL <https://www.sciencedirect.com/science/article/pii/S0005109820303897>.
- [17] Wang, Y., Song, Y., Hill, D. J., and Krstic, M., “Prescribed-Time Consensus and Containment Control of Networked Multiagent Systems,” *IEEE Transactions on Cybernetics*, Vol. 49, No. 4, 2019, pp. 1138–1147. <https://doi.org/10.1109/TCYB.2017.2788874>, URL <https://ieeexplore.ieee.org/document/8272410>.
- [18] Cao, Y., Cao, J., and Song, Y., “Practical prescribed time tracking control over infinite time interval involving mismatched uncertainties and non-vanishing disturbances,” *Automatica*, Vol. 136, 2022, p. 110050. <https://doi.org/10.1016/j.automatica.2021.110050>, URL <https://www.sciencedirect.com/science/article/pii/S0005109821005781>.
- [19] Zhang, K.-K., Zhou, B., and Duan, G.-R., “Global prescribed-time output feedback control of a class of uncertain nonlinear systems by linear time-varying feedback,” *Automatica*, Vol. 165, 2024, p. 111680. <https://doi.org/10.1016/j.automatica.2024.111680>, URL <https://www.sciencedirect.com/science/article/pii/S0005109824001742>.
- [20] Zhao, S., Zheng, J., Yi, F., Wang, X., and Zuo, Z., “Exponential Predefined Time Trajectory Tracking Control for Fixed-Wing UAV With Input Saturation,” *IEEE Transactions on Aerospace and Electronic Systems*, Vol. 60, No. 5, 2024, pp. 6406–6419. <https://doi.org/10.1109/TAES.2024.3402656>, URL <https://ieeexplore.ieee.org/document/10534850/>.

- [21] Xiao, Y., Yang, Y., Ye, D., and Zhao, Y., “Scaling-Transformation-Based Attitude Tracking Control for Rigid Spacecraft With Prescribed Time and Prescribed Bound,” *IEEE Transactions on Aerospace and Electronic Systems*, Vol. 61, No. 1, 2025, pp. 433–442. <https://doi.org/10.1109/TAES.2024.3451454>, URL <https://ieeexplore.ieee.org/document/10659135>.
- [22] Zhou, B., Michiels, W., and Chen, J., “Fixed-Time Stabilization of Linear Delay Systems by Smooth Periodic Delayed Feedback,” *IEEE Transactions on Automatic Control*, Vol. 67, No. 2, 2022, pp. 557–573. <https://doi.org/10.1109/TAC.2021.3051262>, URL <https://ieeexplore.ieee.org/document/9321518>.
- [23] Ding, Y., Zhou, B., Zhang, K.-K., and Michiels, W., “Strong Prescribed-Time Stabilization of Uncertain Nonlinear Systems by Periodic Delayed Feedback,” *IEEE Transactions on Automatic Control*, Vol. 69, No. 6, 2024, pp. 4072–4079. <https://doi.org/10.1109/TAC.2023.3347703>, URL <https://ieeexplore.ieee.org/document/10375772>.
- [24] Zhou, B., Ding, Y., Zhang, K.-K., and Duan, G.-R., “Prescribed time control based on the periodic delayed sliding modesurface without singularities,” *SCIENCE CHINA Information Sciences*, Vol. 67, No. 7, 2024. <https://doi.org/10.1007/s11432-023-4052-4>, URL <https://www.scienceengine.com/10.1007/s11432-023-4052-4>, publisher: Science China Press.
- [25] Kobayashi, H., Shoji, Y., and Yamada, K., “Optimal Attitude Trajectory of Spacecraft with Pyramid-Type CMGs Using a Pseudo-Spectral Method,” *AEROSPACE TECHNOLOGY JAPAN, THE JAPAN SOCIETY FOR AERONAUTICAL AND SPACE SCIENCES*, Vol. 16, No. 0, 2017, pp. 55–63. <https://doi.org/10.2322/astj.16.55>, URL https://www.jstage.jst.go.jp/article/astj/16/0/16_JSASS-D-16-00034/_article/-char/ja/.
- [26] Spiller, D., Melton, R. G., and Curti, F., “Inverse dynamics particle swarm optimization applied to constrained minimum-time maneuvers using reaction wheels,” *Aerospace Science and Technology*, Vol. 75, 2018, pp. 1–12. <https://doi.org/10.1016/j.ast.2017.12.038>, URL <https://www.sciencedirect.com/science/article/pii/S1270963817308684>.
- [27] Celani, F., and Lucarelli, D., “Spacecraft Attitude Motion Planning Using Gradient-Based Optimization,” *Journal of Guidance, Control, and Dynamics*, Vol. 43, No. 1, 2020, pp. 140–145. <https://doi.org/10.2514/1.G004531>, URL <https://arc.aiaa.org/doi/10.2514/1.G004531>, publisher: American Institute of Aeronautics and Astronautics.
- [28] Tao, H. U. O., Jin, Y., Chengfei, Y. U. E., Xueqin, C., and Xibin, C. a. O., “Gradient-based attitude planning for rigid spacecraft on $SO(3)$,” *SCIENCE CHINA Technological Sciences*, Vol. 68, No. 5, 2025. <https://doi.org/10.1007/s11431-024-2883-1>, URL <https://www.scienceengine.com/10.1007/s11431-024-2883-1>, publisher: Science China Press.
- [29] Chai, R., Tsourdos, A., Savvaris, A., Chai, S., Xia, Y., and Chen, C. L. P., “Six-DOF Spacecraft Optimal Trajectory Planning and Real-Time Attitude Control: A Deep Neural Network-Based Approach,” *IEEE Transactions on Neural Networks and Learning Systems*, Vol. 31, No. 11, 2020, pp. 5005–5013. <https://doi.org/10.1109/TNNLS.2019.2955400>, URL <https://ieeexplore.ieee.org/document/8939337>.
- [30] Gong, P., Yan, Z., Zhang, W., and Tang, J., “Lyapunov-based model predictive control trajectory tracking for an autonomous underwater vehicle with external disturbances,” *Ocean Engineering*, Vol. 232, 2021, p. 109010. <https://doi.org/10.1016/j.oceaneng.2021.109010>, URL <https://www.sciencedirect.com/science/article/pii/S0029801821004455>.

- [31] Patterson, M. A., and Rao, A. V., “GPOPS-II: A MATLAB Software for Solving Multiple-Phase Optimal Control Problems Using hp-Adaptive Gaussian Quadrature Collocation Methods and Sparse Nonlinear Programming,” *ACM Trans. Math. Softw.*, Vol. 41, No. 1, 2014, pp. 1:1–1:37. <https://doi.org/10.1145/2558904>, URL <https://dl.acm.org/doi/10.1145/2558904>.